Late Cenozoic evolution of the eastern margin of the Tibetan Plateau: Inferences from $^{40}Ar/^{39}Ar$ and (U-Th)/He thermochronology

Eric Kirby,[1,2] Peter W. Reiners,[3,4] Michael A. Krol,[5] Kelin X. Whipple,[1] Kip V. Hodges,[1] Kenneth A. Farley,[6] Wenqing Tang,[7] and Zhiliang Chen[7]

Received 29 June 2000; revised 20 July 2001; accepted 20 August 2001; published 1 January 2002.

[1] High topography in central Asia is perhaps the most fundamental expression of the Cenozoic Indo-Asian collision, yet an understanding of the timing and rates of development of the Tibetan Plateau remains elusive. Here we investigate the Cenozoic thermal histories of rocks along the eastern margin of the plateau adjacent to the Sichuan Basin in an effort to determine when the steep topographic escarpment that characterizes this margin developed. Temperature-time paths inferred from $^{40}Ar/^{39}Ar$ thermochronology of biotite, multiple diffusion domain modeling of alkali feldspar ^{40}Ar release spectra, and (U-Th)/He thermochronology of zircon and apatite imply that rocks at the present-day topographic front of the plateau underwent slow cooling (<1°C/m.y.) from Jurassic times until the late Miocene or early Pliocene. The regional extent and consistency of thermal histories during this time period suggest the presence of a stable thermal structure and imply that regional denudation rates were low (<0.1 mm/yr for nominal continental geotherms). Beginning in the late Miocene or early Pliocene, these samples experienced a pronounced cooling event (>30°–50°C/m.y.) coincident with exhumation from inferred depths of ~8–10 km, at denudation rates of 1–2 mm/yr. Samples from the interior of the plateau continued to cool relatively slowly during the same time period (~3°C/m.y.), suggesting limited exhumation (1–2 km). However, these samples record a slight increase in cooling rate (from <1 to ~3°C/m.y.) at some time during the middle Tertiary; the tectonic significance of this change remains uncertain. Regardless, late Cenozoic denudation in this region appears to have been markedly heterogeneous, with the highest rates of exhumation focused at the topographic front of the plateau margin. We infer that the onset of rapid cooling at the plateau margin reflects the erosional response to the development of regionally significant topographic gradients between the plateau and the stable Sichuan Basin and thus marks the onset of deformation related to the development of the Tibetan Plateau in this region. The present margin of the plateau adjacent to and north of the Sichuan Basin is apparently no older than the late Miocene or early Pliocene (~5–12 Ma). *INDEX TERMS:* 8110 Tectonophysics: Continental tectonics-general (0905), 9320 Information related to geographic region: Asia, 8102 Tectonophysics: Continental contractional orogenic belts; *KEYWORDS:* Tibetan Plateau, thermochronology, denudation, relief

1. Introduction

[2] The question of when the Tibetan Plateau attained its current elevation, and how rapidly it did so, is at the forefront of debate over a wide range of first-order problems in continental tectonics. For example, the timing of plateau development places important constraints on the mechanism(s) by which convergence between India and Eurasia has been accommodated [*Tapponnier et al.*, 1982; *England and Houseman*, 1986], while the rates of uplift of the plateau surface have major implications for the dynamics of plateau formation and the relative significance of deformational processes in the crust and mantle [*England and Molnar*, 1990]. The development of high elevation in central Asia has been linked to the onset and intensification of the Asian monsoon [*Molnar et al.*, 1993] and perhaps to the drawdown of atmospheric CO_2 via enhanced silicate weathering [*Raymo et al.*, 1988]. Thus the elevation history of the Tibetan Plateau plays a central role in the continuing debate over large-scale linkages between tectonics and global climate change.

[3] Despite the importance of the timing and rate of plateau development, there is little direct evidence for when and how rapidly uplift of the Tibetan plateau occurred [*Molnar et al.*, 1993]. Current estimates for when the plateau attained its current elevation are based on inferences regarding the initiation age of E-W extension in central and southern Tibet [*Harrison et al.*, 1992; *Coleman and Hodges*, 1995] or of bimodal, potassic volcanism in north central Tibet [*Turner et al.*, 1993, 1996; *Chung et al.*, 1998; *Hacker et al.*, 2000]. Both of these tectonic events are linked to a model for uplift of the plateau surface involving convective removal of a thickened continental lithosphere [*Houseman et al.*, 1981; *Molnar et al.*, 1993; *Lenardic and Kaula*, 1995]. Although simple geodynamic models linking surface uplift, potential energy increase in the lithosphere, extension, and volcanism are conceptually compelling, a temporal and genetic link between extension, volcanism, and surface uplift remains to be demonstrated. Furthermore, the cause of E-W extension on the high plateau is a matter of active debate; it may be related to a number of processes including strain partitioning during oblique convergence [*McCaf-*

[1]Department of Earth, Atmospheric, and Planetary Science, Massachusetts Institute of Technology, Cambridge, Massachusetts, USA.
[2]Now at Institute for Crustal Studies, University of California, Santa Barbara, California, USA.
[3]Department of Geology, Washington State University, Pullman, Washington, USA.
[4]Now at Department of Geology and Geophysics, Yale University, New Haven, Connecticut, USA.
[5]Department of Earth Sciences, Boston University, Boston, Massachusetts, USA.
[6]Department of Geological and Planetary Sciences, California Institute of Technology, Pasadena, California, USA.
[7]Chengdu Institute of Geology and Mineral Resources, Chengdu, Sichuan, P.R. China.

0278-7407/02/2000TC001246$12.00

frey and Nabelek, 1998], spreading of the Himalayan arc [*Seeber and Pecher*, 1998], eastward extrusion of Tibet [*Armijo et al.*, 1986], or thickening of crust with a depth-dependent rheology [*Royden*, 1996].

[4] Rather than envisioning plateau uplift as a spatially and temporally uniform event, a second class of models holds that the plateau grew in lateral extent (primarily to the east) with continuing convergence between India and Eurasia [*England and Houseman*, 1986, 1988; *Royden*, 1996]. The deformational history of the Qaidam-Qilian Shan region of Qinghai Province seems to support the inference that shortening and crustal thickening has stepped northward with time [*Meyer et al.*, 1998]. However, this region is characterized by high mountain ranges and intermontane basins, and it may have a tectonic and topographic history independent of the plateau to the south. Although it has been suggested recently that portions of southern Tibet had already attained high elevations prior to the Indo-Asian collision [*Murphy et al.*, 1997], there is virtually no information on how surface uplift of the plateau varied in space and time. To begin to comprehensively address this question, one must first determine when the present margins of the plateau developed.

[5] In this contribution, we investigate the rates and pattern of Cenozoic denudation along the eastern margin of the Tibetan Plateau adjacent to the Sichuan Basin (Figure 1). The topographic margin of the plateau in this region is a 4–5 km high escarpment defined by steep, consequent drainages eroding headward into an unincised plateau surface of low relief. The development of this high topography presents something of an enigma in that shortening of the upper crust during the Cenozoic appears to be rather limited [*Burchfiel et al.*, 1995]. This observation, coupled with the absence of a Cenozoic foredeep in the Sichuan Basin and slow geodetic rates of shortening between the plateau and the Sichuan Basin [e.g., *Chen et al.*, 2000], led *Royden et al.* [1997] to suggest that the development of the plateau in eastern Tibet was the consequence of thickening and flow within a weak lower crust. Thus, in addition to addressing the regional question of when the eastern plateau developed, estimates of the magnitude and distribution of exhumation across this margin will place first-order constraints on the degree of upper crustal deformation in this region.

2. Morphology of the Eastern Margin

[6] In contrast to the northern and southern margins of the Tibetan Plateau, the topographic expression of most of the eastern margin is irregular and diffuse. In southeastern Tibet, between the eastern syntaxis of the Himalaya and the Sichuan Basin, the plateau has no distinct topographic margin. Elevations decrease gradually from >5000 m to <1000 m over hundreds of kilometers; this topographic gradient has been interpreted as the consequence of flow of weak lower crust from beneath the high plateau [*Clark and Royden*, 2000]. In the Longmen Shan region, however, the topographic margin of the Tibetan Plateau is one of the world's most remarkable continental escarpments (Figure 1). Elevations rise from ~600 m in the southern Sichuan Basin to peaks exceeding 6500 m over a horizontal distance of <50 km. Regional topographic gradients typically exceed 10% along this mountain front and rival any other margin of the plateau. To the north, peak elevations decrease somewhat, but regional slopes remain steep, rising from ~700 m to nearly 5000 m in 30–40 km. At the northwest corner of the Sichuan Basin the topographic front of the plateau turns north and transects the E-W trending Qinling Mountains. The margin is defined in this region by a high mountain range, the Min Shan, which marks the transition from plateau elevations of ~4000 m to elevations between 1000 and 1500 m in the western Qinling Shan. Peak elevations in the Min Shan exceed 5500 m. North of the Min Shan the topographic margin of the plateau is diffuse; plateau elevations gently grade into regional elevations near 1000 m.

[7] The steep topographic escarpment adjacent to the Sichuan Basin has been deeply dissected by several major rivers; local valley-ridge top relief in many places along the escarpment exceeds 3000 m (Figure 1). These rivers are short, steep bedrock channels that ultimately flow across the Sichuan Basin into the Chang Jiang (Yangtze River). Although some of the rivers west and southwest of the Sichuan Basin have their headwater regions in the central plateau, rivers draining the Longmen Shan escarpment extend <200 km westward. Along the northern portion of the margin, west of the Min Shan, rivers draining into the Sichuan Basin are actively eroding headward into the plateau surface, and recent stream captures are evident in the drainage pattern and stream gradients [*Kirby and Whipple*, 2000]. Along the southern portion of the margin drainage divides are set by a competition between rivers draining the eastern escarpment, and tributaries of the Dadu Jiang, a major south flowing river west of the margin (Figure 1).

[8] The surface of the plateau north and west of the escarpment stands at elevations between 3500 and 4000 m (Figure 1) and is characterized by extremely low local relief (200–300 m). The landscape atop the plateau slopes gently to the west-northwest, and rivers draining this region flow generally northwest into the Huang He (Yellow River). Although some authors have recently proposed that the low relief of the central plateau is the consequence of backfilling of terrestrial basins behind active mountain ranges [*Meyer et al.*, 1998], there is little evidence of this process in eastern Tibet. Large contiguous regions (>10^5 km^2) of low relief are developed on pre-Cenozoic bedrock (Figure 1), and Cenozoic terrestrial sediments are rare and restricted to the vicinity of the Yellow River [*Ministry of Geology and Mineral Resources*, 1991] (Figure 2). The timing of development and the subsequent evolution of this low-relief landscape are essentially unknown.

[9] The eastern margin of the Tibetan Plateau adjacent to the Sichuan Basin appears to be an erosional escarpment formed in response to development of regional elevation gradients between the plateau and the Sichuan Basin. As the Sichuan Basin has remained relatively stable throughout the Cenozoic [*Burchfiel et al.*, 1995], the timing and degree of exhumation along this escarpment can place important constraints on the rates and patterns of deformation in this region of the plateau.

3. Tectonic Setting of the Longmen Shan Region

[10] The eastern margin of the Tibetan Plateau in the vicinity of the Sichuan Basin coincides with the Longmen Shan thrust belt, a feature developed along the western margin of the Yangtze craton in Mesozoic time and reactivated in the Cenozoic [*Dirks et al.*, 1994; *Burchfiel et al.*, 1995]. Although the focus of this paper is on

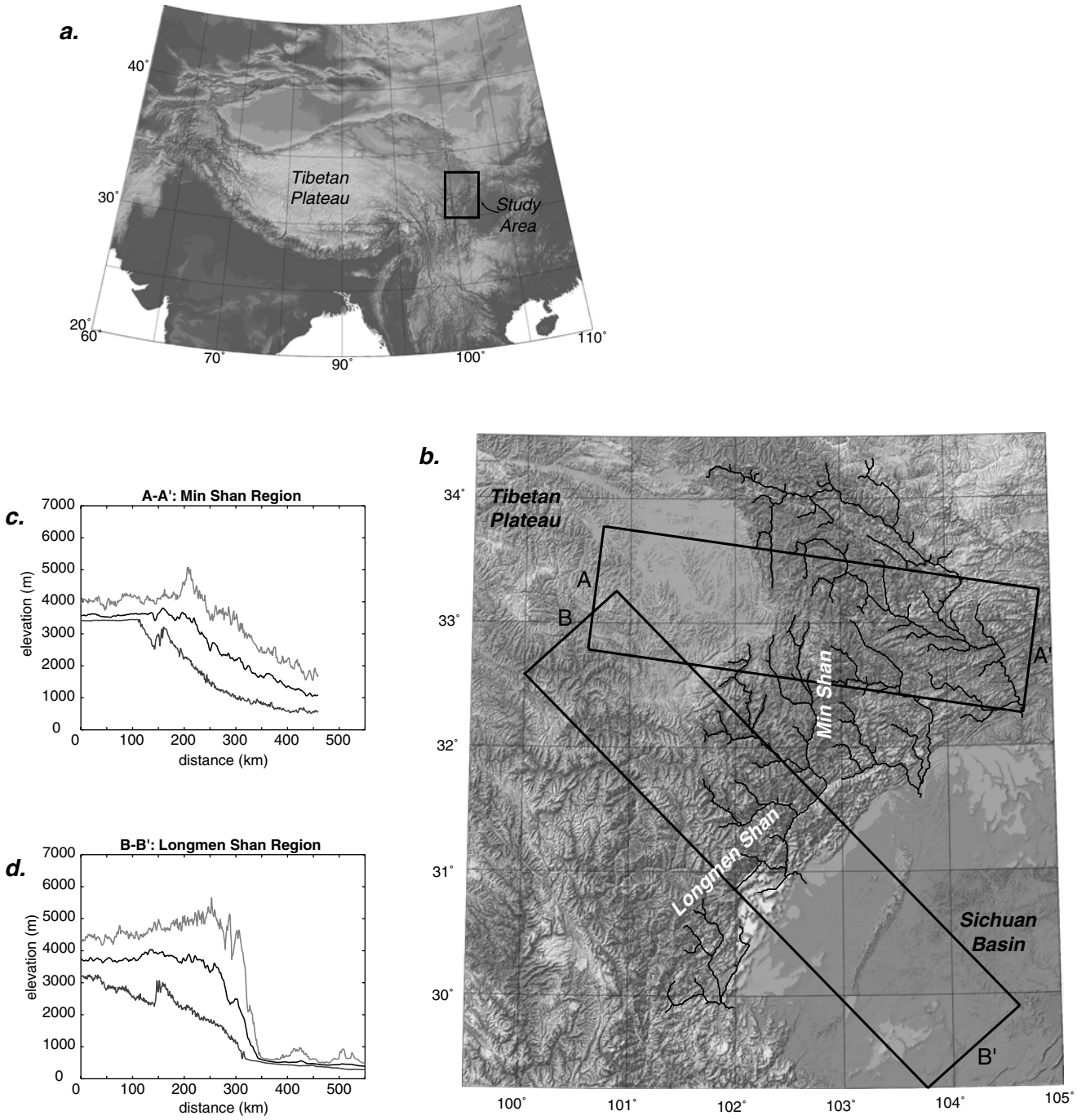

Figure 1. Regional morphology of the eastern margin of the Tibetan Plateau adjacent to the Sichuan Basin. (a) Index shaded relief image of the Indo-Asian collision zone. Box shows approximate location of the study area. (b) Shaded relief image of the eastern margin. Note the deeply dissected, high-relief escarpment along the margin. Major rivers draining the escarpment are overlain in bold and serve to illustrate the approximate location of the drainage divide. Locations of swath-averaged topographic profiles are shown as rectangular boxes. (c and d) Swath-averaged topography across the eastern margin in the Min Shan and Longmen Shan regions, respectively. Topography was extracted in a 100 km wide, rectangular swath and projected onto a vertical plane located at the midline of the swath. Shown are maximum, mean, and minimum elevations for each swath. Note the remarkably steep topographic front along the Sichuan Basin, and the somewhat more moderate front north of the basin.

the Cenozoic thermal evolution of rocks along the eastern margin, our results have important implications for the Mesozoic tectonic history of this region as well. In this section we briefly summarize salient aspects of the geology of the Longmen Shan region, discuss the Mesozoic tectonic history, and provide an overview of the Cenozoic tectonics. For a more complete treatment of the geology of this complex region, see *Burchfiel et al.* [1995].

3.1. Geology of the Longmen Shan

[11] For simplicity of discussion we divide the geology of the Longmen Shan region into four distinct tectonostratigraphic packages (Figure 2). From oldest to youngest, these include the following: (1) crystalline basement rocks of the Yangtze craton, (2) Neoproterozoic-Permian passive margin sediments, (3) Triassic flysch of the Songpan-Garze terrane, and (4) Mesozoic-Cenozoic terrestrial sediments in the Sichuan Basin. These packages are juxtaposed across a series of structures with polyphase histories, collectively termed the Longmen Shan Thrust Belt [*Dirks et al.*, 1994; *Burchfiel et al.*, 1995]. We describe each of these components and their structural relations in this section.

[12] Crystalline rocks of the Yangtze craton are exposed in a belt of basement massifs adjacent to the southwest corner of the Sichuan Basin (Figure 2). The massifs consist of quartzofeldspathic gneisses and associated granitoids that are thought to be Precambrian [*Ministry of Geology and Mineral Resources*, 1991]. They are structurally overlain by a parautochthonous passive margin sequence, and thus assumed to represent the basement of the Yangtze craton. The passive margin sequence itself consists primarily of shallow water marine rocks of Neoproterozoic (Sinian) to Permian age. Permian carbonates generally grade into deep-water deposits of the Songpan-Garze terrane (Figure 2), a $\sim$500,000 km^2 region of vertically dipping, isoclinally folded Triassic flysch and graywacke that may represent incomplete closure of a Paleotethyan ocean basin [*Sengor et al.*, 1993; *Zhou and Graham*, 1996].

[13] All three tectonostratigraphic packages were deformed during Mesozoic time as evident in a series of east directed thrusts that place the Neoproterozoic-Triassic passive margin sequence atop the craton [*Chen and Chen*, 1987; *Chen et al.*, 1994a; *Dirks et al.*, 1994; *Burchfiel et al.*, 1995; *Chen and Wilson*, 1996]. The thrust belt trends northeast and merges with the E-W trending Qinling orogen [*Mattauer et al.*, 1985] north of the Sichuan Basin. Northwest trending folds within the Songpan-Garze wrap into parallelism with the western edge of the Longmen Shan thrust belt (Figure 2), and likely indicate that the thrust belt had a significant sinistral component during Mesozoic transpressional deformation [*Dirks et al.*, 1994; *Burchfiel et al.*, 1995].

[14] Substantial metamorphism and plutonism accompanied Mesozoic deformation in the Longmen Shan region. Metamorphic grade of the passive margin sequence ranges from negligible to lower amphibolite and generally increases toward the hinterland [*Dirks et al.*, 1994; *Burchfiel et al.*, 1995]. Metamorphism was accompanied by emplacement of a suite of Mesozoic plutons (generally granodiorite to monzonite) into the Triassic flysch northwest of the thrust belt [*Roger et al.*, 1995b]. These plutons are generally macroscopically undeformed and cut across isoclinal, upright folds within the flysch. Contact metamorphic mineral assemblages from the flysch adjacent to the plutons include andalusite and cordierite [*Dirks et al.*, 1994], suggesting that the plutons were emplaced at pressures $<2.5-3$ kbar [*Bohlen et al.*, 1991]. Contact metamorphic minerals overgrow regional fabrics within the flysch, and, combined with the undeformed nature of the granitoids themselves, suggest that most of the plutons were emplaced late in the deformational history [*Dirks et al.*, 1994].

[15] The fourth tectonostratigraphic package in the region consists of terrestrial sediments east of the thrust belt. Triassic-Cretaceous sediments comprise westward thickening wedges of fluvial mudstones, sandstones, and conglomerates deposited in an flexural basin in front of the thrust belt [*Chen et al.*, 1994a; *Burchfiel et al.*, 1995]. Total thickness of these deposits locally exceeds 10 km [*Burchfiel et al.*, 1995]. Cenozoic sediments, however, are restricted to the southwest corner of the basin and consist of a thin (<700 m) sequence of terrestrial fluvial and lacustrine deposits.

3.2. Mesozoic Tectonics of the Longmen Shan

[16] Mesozoic deformation in the Longmen Shan thrust belt is reflected in major changes in depositional patterns along the western margin of the Sichuan Basin. Lower and Middle Triassic rocks atop the Yangtze craton are shallow marine to nonmarine in character. Rapid deposition of terrestrial deposits (up to several kilometers) began in the Late Triassic [*Burchfiel et al.*, 1995]. East directed thrust sheets in the Longmen Shan (Tangwangzhai nappe, Figure 2) carry Paleozoic passive margin rocks above uppermost Triassic and Lower Jurassic terrestrial sediments in the Sichuan Basin [*Chen et al.*, 1994a]. In several localities east of the Min Shan (Figure 2) these faults are overlapped by Early and Middle Jurassic basin fill that narrowly restricts the timing of deformation along the thrust front [*Burchfiel et al.*, 1995].

[17] Within the Songpan-Garze terrane to the west, the Lower and Middle Triassic is characterized by deep marine deposition, with a rapid influx of turbidites and flysch beginning in the Middle Triassic [*Burchfiel et al.*, 1995]. By Late Triassic time, the basin had shallowed, and coal-bearing clastics were deposited locally. Although all of these units were severely deformed and imbricated during basin closure in the latest Triassic [*Zhou and Graham*, 1996], the preservation of this uppermost basin fill suggests that the Mesozoic tectonism within the Songpan-Garze did not create high mountains subject to significant erosion [*Burchfiel et al.*, 1995].

[18] There is little direct evidence for late Middle Jurassic to Cretaceous deformation within the Longmen Shan region, although westward thickening wedges of conglomerates of this age indicate continued subsidence along the foredeep [*Burchfiel et al.*, 1995]. *Arne et al.* [1997] obtained Late Cretaceous ^{40}Ar/^{39}Ar ages (circa $120-130$ Ma) from muscovites in metamorphic rocks northwest of the Wenchuan-Maowen fault. Although they interpreted these ages as reflecting differential cooling across this shear zone, the extent of Late Cretaceous deformation in the Longmen Shan remains essentially unknown.

3.3. Cenozoic Tectonics of the Longmen Shan

[19] Despite the impressive topographic front along the Longmen Shan, shortening across this margin of the plateau appears to have been relatively minor during Cenozoic time. The lack of a Cenozoic foredeep along in the Sichuan Basin indicates that flexural loading of the basin was negligible during formation of the plateau [*Burchfiel et al.*, 1995; *Royden et al.*, 1997]. In

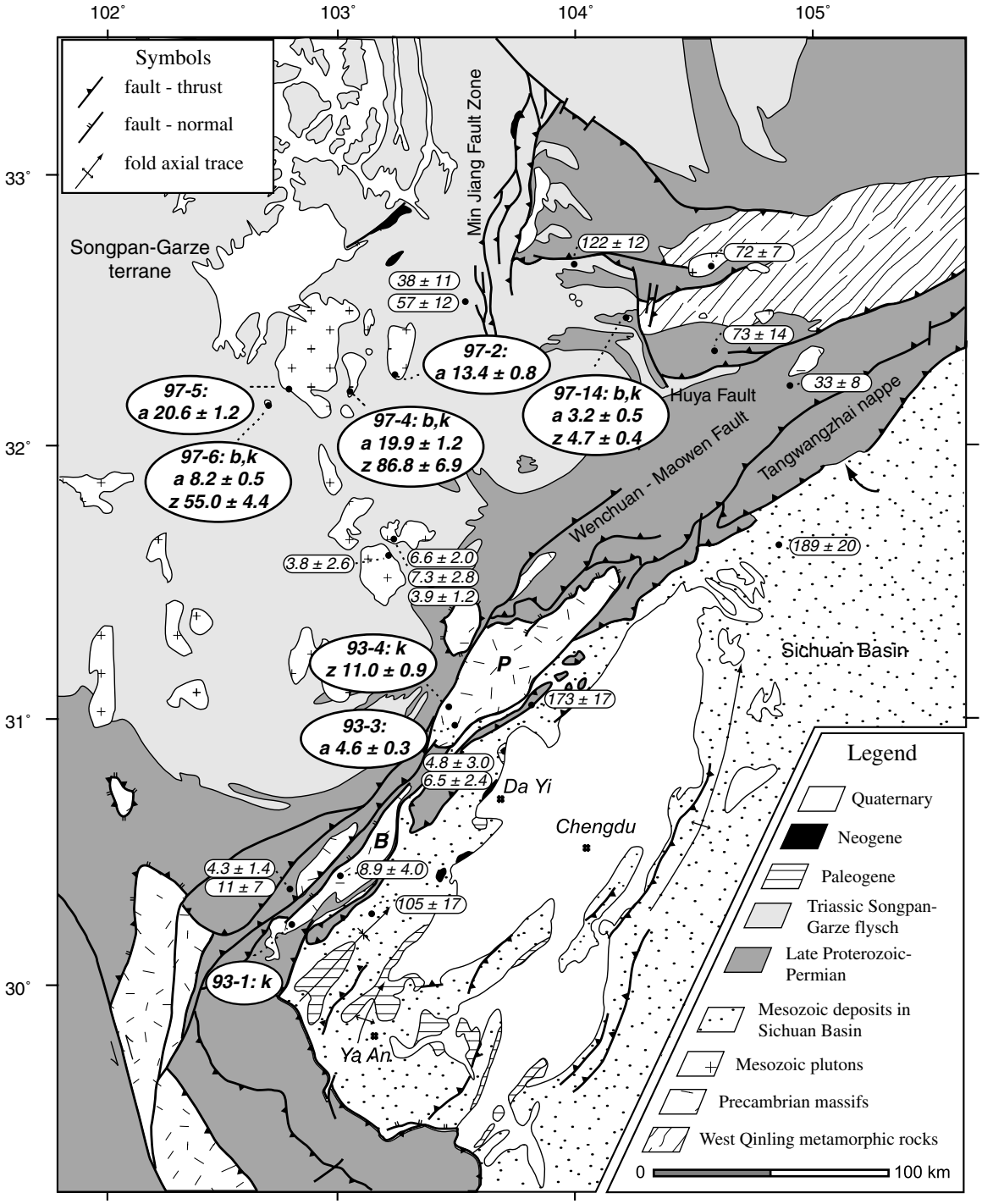

Figure 2. Simplified geologic map of the Longmen Shan region of the eastern margin of the Tibetan Plateau. Geology modified after *Burchfiel et al.* [1995], 1:200,000 geologic maps [*Ministry of Geology and Mineral Resources*, 1991], and our own observations. Names of selected cities, major structures, and geographic regions are shown for reference to the text: P, Pengguan Massif; B, Baoxing Massif. Arrow highlights region where Jurassic terrestrial sediments overlap frontal thrust faults along the Tangwangzhai Nappe. Large ellipses show the sample locations and (U-Th)/He apatite ages of this study (z, zircon; a, apatite). Shown for reference in small ellipses are apatite fission track age determinations of *Arne et al.* [1997].

addition, space geodetic studies indicate that active shortening across the Longmen Shan is less than a few mm/yr and within uncertainty of zero [*King et al.*, 1997; *Chen et al.*, 2000]. Significant tilting of Pleistocene-Recent markers is present within the western Min Shan, a N-S trending range along the margin of the plateau north and west of the Sichuan Basin (Figure 2) [*Tang et al.*, 1993; *Chen et al.*, 1994b; *Kirby et al.*, 2000], yet it occurs in the absence of resolvable E-W shortening between the plateau and the basin [*Kirby et al.*, 2000].

[20] Some Cenozoic deformation is present in the southern Longmen Shan and has important implications for the timing of tectonism along this margin of the plateau. In the southwestern Sichuan Basin, a series of NE trending folds involve Cretaceous-Oligocene rocks and are overlapped by flat-lying Neogene sediments (Figure 2). A belt of Paleozoic klippen was emplaced above folds in Upper Jurassic rocks that are continuous with the rocks below the Cenozoic section [*Burchfiel et al.*, 1995]. These relationships indicate that some shortening occurred after the Oligocene, but the exact timing is unknown. Facies relationships between the klippen and units further west suggest that Cenozoic shortening in the southern Longmen Shan region is less than a few tens of kilometers [*Burchfiel et al.*, 1995].

[21] The degree of Cenozoic deformation west of the klippen is unknown, although shortening appears to be relatively minor [*Dirks et al.*, 1994; *Burchfiel et al.*, 1995]. Interestingly, a belt of normal faults occurs along the western margin of the Precambrian massifs [*Burchfiel et al.*, 1995]. These faults are characterized by low-grade mylonitic textures with kinematic indicators that suggest west side down displacement. These faults may be continuous with similar structures along the thrust belt to the southwest (Figure 2). $^{40}Ar/^{39}Ar$ cooling ages from micas within these mylonites range from Cretaceous to mid-Tertiary (circa 25–30 Ma) [*Hames and Burchfiel*, 1993], and the authors interpreted the youngest of these ages as a best estimate of the timing of normal faulting.

[22] *Arne et al.* [1997] interpreted fission track age variations in zircon and apatite across the Longmen Shan thrust belt as indicating differential cooling in response to Cenozoic reactivation of Mesozoic structures. Zircon fission track ages west of the Wenchuan-Maowen fault range from 38 to 68 Ma, while a single sample east of the fault yielded an age of 110 Ma. Apatite fission track ages are typically late Miocene within the thrust belt and appear to be invariant across the Wenchuan-Maowen fault [*Arne et al.*, 1997] (Figure 2). Apatites from Mesozoic terrestrial deposits in the Sichuan Basin yield fission track ages between 93 and 189 Ma, in all cases near the depositional age of the sediments [*Arne et al.*, 1997]. In the Min Shan region, apatites yielded ages ranging from circa 120 to 70 Ma. Track length models from these three samples suggest an increase in cooling rates sometime after circa 20 Ma, that the authors interpret to reflect the inception of deformation in this region of the plateau [*Arne et al.*, 1997].

4. Thermal History of the Longmen Shan Region

[23] To better resolve the Cenozoic thermal history of this region of the Tibetan Plateau, we utilized a variety of thermochronometers including $^{40}Ar/^{39}Ar$ in biotite and potassium feldspar, and (U-Th)/He in zircon and apatite. Details of the analytical procedures are presented in Appendix A. Nominal closure temperatures in these systems range from ~300°–350°C (biotite) [*Grove and Harrison*, 1996] to ~70°C (apatite) [*Farley*, 2000], and multidiffusion domain modeling of K-feldspar $^{40}Ar/^{39}Ar$ spectra [*Lovera et al.*, 1989] permits exploration of much of the temperature interval in between. Furthermore, the closure temperature for He diffusion in zircon ranges from ~160°–210°C [*Reiners et al.*, 2002] and allows for an independent check on the reliability of the feldspar thermal models. Our sampling strategy was designed to test for possible spatial variations in the Cenozoic thermal history across a large geographic region. We chose to examine a suite of thermochronometers within each sample rather than utilize the age-elevation relationship of a single system because little information is available in eastern Tibet to effectively guide the latter approach. We collected three samples from the margin of the plateau. Two of these are from Precambrian massifs (Pengguan and Baoxing massifs; see Figure 2) along the margin adjacent to the Sichuan Basin, while one is from a Mesozoic pluton along the eastern foot of the Min Shan (Figure 2). We also collected four samples from the interior of the plateau, in the headwater reaches of one of the primary rivers in this region, the Hei Shui He (Black Water River). These four samples are from Mesozoic plutons within the Songpan-Garze terrane west of the thrust belt (Figure 2). We collected samples from the valley floors east of the drainage divide and from the low relief surface west of the divide, spanning ~2 km of relief.

4.1. $^{40}Ar/^{39}Ar$ Results—Biotite

[24] We obtained biotite separates from three granitoid plutons within the Songpan-Garze terrane. Samples EK 97-4 and 97-6 were collected from plutons in the headwaters of the Hei Shui He, while sample EK 97-14 was collected from a small (~3 km^2) stock at the eastern foot of the Min Shan (Figure 2). Incremental heating of these samples yielded relatively straightforward release spectra (Figure 3), but no statistically defined plateaux. Moreover, the highly radiogenic nature of the ^{40}Ar in the samples prevented their evaluation for possible excess ^{40}Ar contamination [*Roddick et al.*, 1980]. Our best estimates of the $^{40}Ar/^{39}Ar$ closure ages of these biotites are the ^{39}Ar weighted means of the dates for increments defining relatively flat portions of the spectra: ~194 Ma for 97-4, ~208 Ma for 97-6, and ~171 Ma for 97-14. Although provisional, these dates are consistent with emplacement ages determined for similar plutons in the Songpan-Garze terrane to the south [*Roger et al.*, 1995b], and probably record rapid cooling of the plutons following emplacement.

4.2. $^{40}Ar/^{39}Ar$ Results—K-Feldspar

[25] To resolve the thermal history of the Longmen Shan region between the Jurassic ages recorded in biotites and Miocene-Pliocene ages recorded in apatites (in Section 4.3), we analyzed potassium feldspars from five samples distributed across the plateau and modeled the results following the multiple diffusion domain (MDD) theory [*Lovera et al.*, 1989, 1991]. Whether or not this model accurately represents radiogenic ^{40}Ar diffusion in natural feldspars over geologic timescales is controversial [*Parsons et al.*, 1988; *Villa*, 1994; *Parsons et al.*, 1999]. Persuasive as the mineralogical arguments against the MDD model may be, the fact remains that numerous applications of the method to samples from a variety of geologic settings have yielded sensible time-temperature paths that seem consistent with independent thermochronologic constraints [*Arnaud*

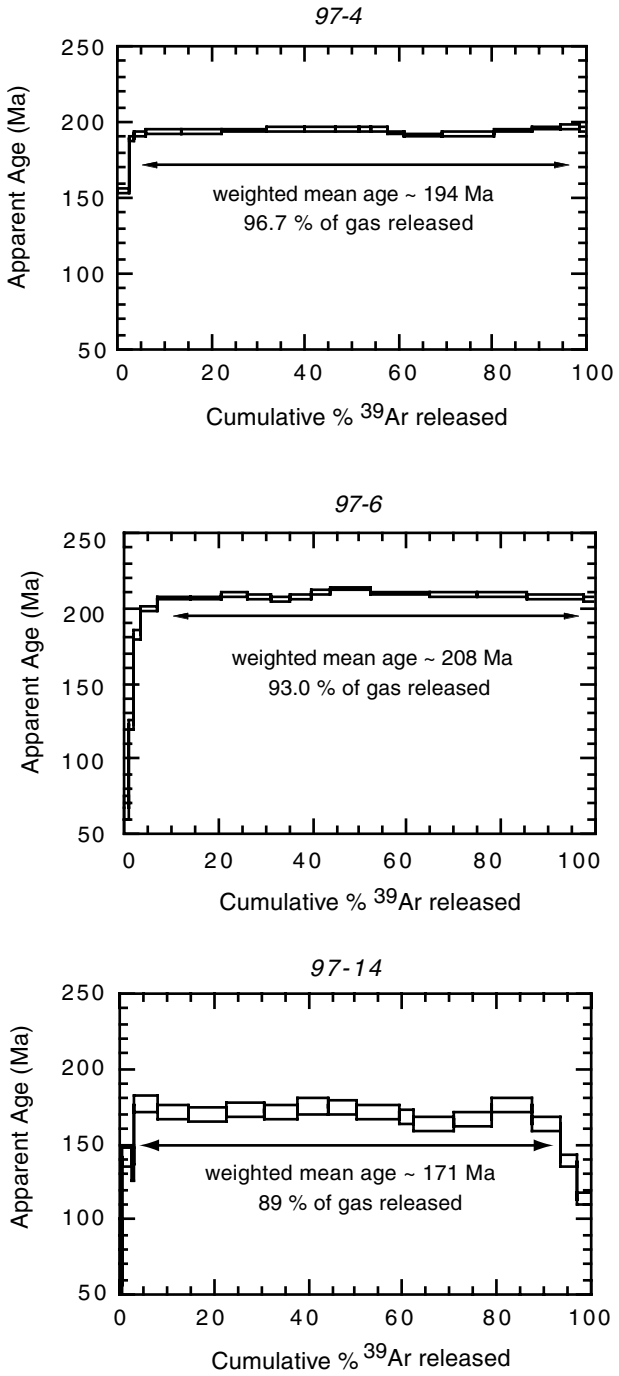

Figure 3. Biotite $^{40}Ar/^{39}Ar$ release spectra for samples from granitoid plutons in the region. Arrows show the range of steps used in the weighted mean age calculation.

et al., 1993; *Leloup et al.*, 1993; *Krol et al.*, 1996; *Warnock and Zeitler*, 1998]. Our approach has been to proceed with the modeling exercise and ask, whenever possible, whether the modeled temperature-time path is consistent with the higher- and lower-temperature constraints provided by the $^{40}Ar/^{39}Ar$ and (U-Th)/He data.

[26] The interpretation of the $^{40}Ar/^{39}Ar$ results in terms of the MDD model requires some assumption regarding the general form of the temperature-time path experienced by the samples [*Lovera et al.*, 1989]. We restrict our models to the simplest possible solution, monotonic cooling. Transient reheating could significantly alter the interpretation of the thermal history. However, we are confident that we can discount the possibility of Cenozoic reheating for a variety of reasons. First, there is no evidence for Cenozoic magmatism in this region of eastern Tibet; all dated plutons within the study area are Mesozoic [*Roger et al.*, 1995b]. The only recognized Cenozoic pluton is exposed in the Gongga Shan massif [*Roger et al.*, 1995a], well south and west of the Sichuan Basin. Second, geothermal activity is very limited in this region of the plateau. Finally, preliminary analyses of fission track length distributions in samples from the northern portion of the margin (Min Shan) suggest slow cooling during the late Mesozoic and early Cenozoic [*Arne et al.*, 1997]. Thus we feel that monotonic cooling is a reasonable first-order interpretation of the feldspar $^{40}Ar/^{39}Ar$ results. As discussed in section 4.2.3, it appears to work in all cases but one.

[27] Feldspars from the Longmen Shan region show differences in age and thermal history that appear to correspond with the location of the samples relative to the plateau margin. We first discuss samples collected from the margin adjacent to and north of the Sichuan Basin (93-4, 97-14), one from the southern Longmen Shan (93-1), and then turn to samples from the interior of the plateau (97-4, 97-6).

4.2.1. Plateau margin. [28] Measured age spectra for samples 93-4 and 97-14 are presented in Figures 4a and 5a, respectively. Both samples are characterized by saddle-shaped release spectra that suggest the presence of excess argon in the low-temperature release steps. Duplicate isothermal heating increments [*Harrison et al.*, 1994] permitted the isolation of late Miocene components of gas released early in the experiments. The ages of subsequent steps increase monotonically to maxima of ~147 Ma (93-4) and ~61 Ma (97-14). However, the spectra of sample 93-4 is complicated by the apparent presence of excess argon between 15 and 25% of gas released (Figure 4a). It is possible that the low-temperature steps (5–15% of gas released) are also contaminated with excess argon, and these should be considered maximum ages (circa 11–12 Ma). Diffusion parameters (activation energy, $E_a$and frequency factor, D_o/r^2) calculated from the release of ^{39}Ar are presented in Figures 4b and 5b and are typical of alkali feldspars [*Lovera et al.*, 1997]. The domain size distribution for each sample is shown in Figures 4c and 5c.

[29] Model temperature-time paths (inverted from the release spectra and kinetic parameters; see Appendix A) are shown in Figures 4d and 5d. Both thermal histories are remarkably similar and suggest that the samples underwent extremely slow cooling during the Cretaceous and early Tertiary. The modeled cooling curve for 97-14 is poorly constrained by data at temperatures higher than ~240°C, but a simple extrapolation of the nearly linear portion of the curve (between ~200° and 240°C) to older ages is consistent with closure for ^{40}Ar in biotite [*Grove and Harrison*, 1996] having been achieved at ~171 Ma, the approximate age of biotite from this sample. Modeled cooling curves show a dramatic increase in cooling rates (~20°–50°C/m.y.) during the late Miocene beginning at 11–12 Ma for sample 93-4 and 6-7 Ma for sample 97-14.

4.2.2. Plateau interior. [30] In contrast to samples from the topographic margin, feldspars collected from Mesozoic plutons in

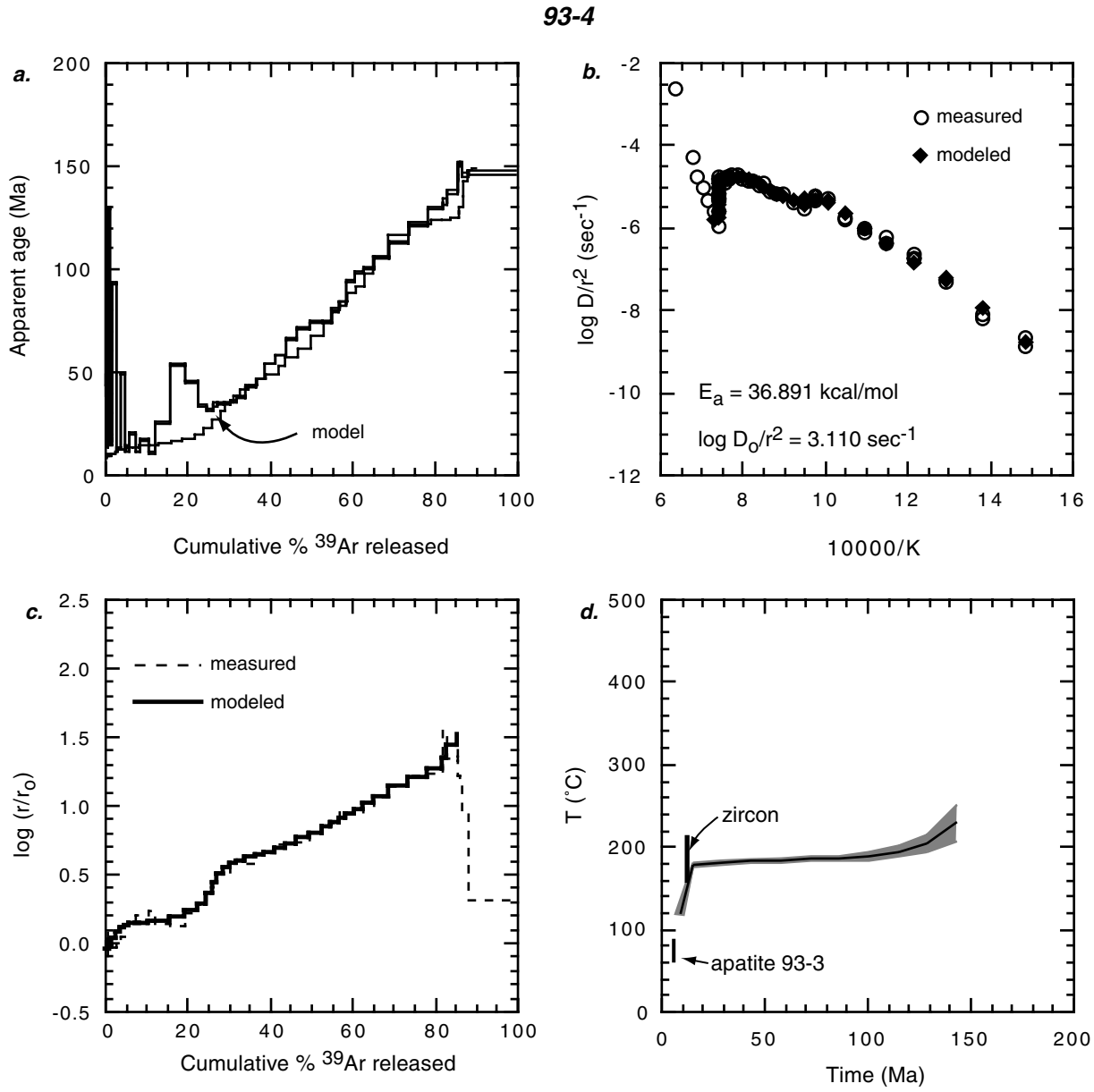

Figure 4. (a) $^{40}Ar/^{39}Ar$ release spectrum (open boxes) and mean of 100 modeled age spectra (solid line) for alkali feldspar collected from the Pengguan massif, adjacent to the Sichuan Basin. (b) Arrhenius plot of log D/r^2 versus reciprocal temperature. Arrhenius data are calculated assuming plane slab diffusion geometry from measured ^{39}Ar release during incremental heating experiment. (c) Plot of log (r/r_o) versus ^{39}Ar released (dashed line) and theoretical fit (solid line) from model. (d) Model thermal history for sample 93-4 obtained from inverse modeling of the kinetic parameters and domain structure. Shaded region represents the range of 100 best fit model results. Solid line is the mean. Note the agreement between the modeled thermal history and (U-Th)/He results from zircon and apatite (sample 93-3).

the headwaters of the Hei Shui He (Figure 2) yielded minimum ages of ~50–70 Ma (Figures 6a and 7a, samples 97-4 and 97-6, respectively). Minor excess ^{39}Ar was apparent in the first 5–10% of the gas released. The measured ages increase monotonically from the minimum to ~195–210 Ma. The diffusion behavior of these samples was slightly more complex than that of samples from the topographic margin. For example, duplicate isothermal steps for sample 97-4 display a systematic offset resulting in two subparallel arrays on an Arrhenius diagram (Figure 6b). We attribute this behavior to a slight hystersis in the temperature cycling that appears to be a consequence of our heating schedule for this sample (see supporting data Table A1, which is available as an electronic supplement[1]). Because the furnace had more time to

[1] Supporting Table A1 is available via Web browser or via Anonymous FTP from ftp://kosmos.agu.org, directory "append" (Username = "anonymous," Password = "guest"); subdirectories in the ftp site are arranged by paper number. Information on searching and submitting electronic supplements is found at http://www.agu.org/pubs/esupp_about.html.

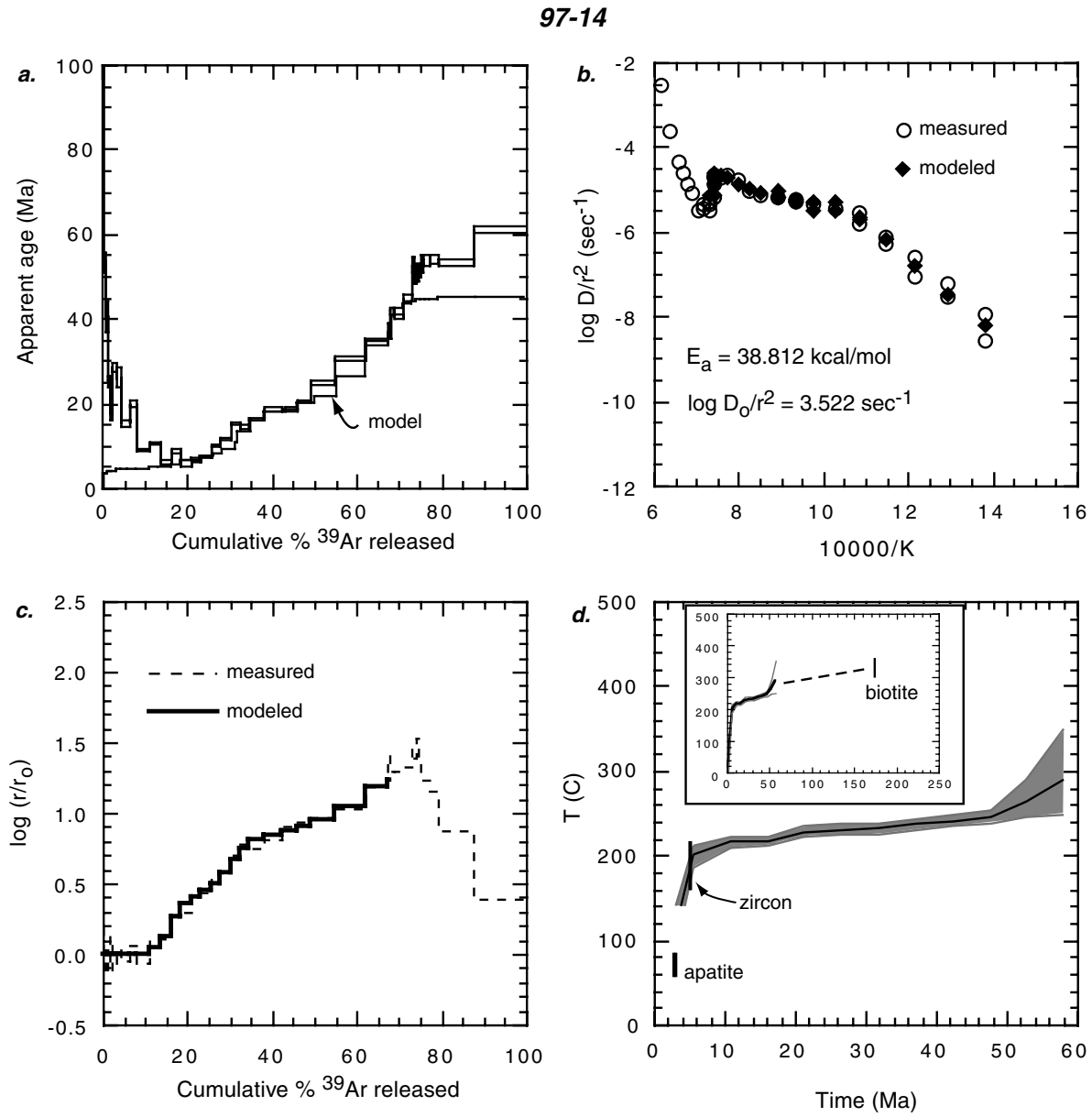

Figure 5. (a) $^{40}Ar/^{39}Ar$ release spectrum (open boxes) and mean of 100 modeled age spectra (solid line) for alkali feldspar collected from the eastern flank of the Min Shan, north of the Sichuan Basin. (b) Arrhenius plot of log D/r^2 versus reciprocal temperature. Arrhenius data are calculated assuming plane slab diffusion geometry from measured ^{39}Ar release during incremental heating experiment. (c) Plot of log (r/r_o) versus ^{39}Ar released (dashed line) and theoretical fit (solid line) from model. (d) Model thermal history for sample 97-14 obtained from inverse modeling of the kinetic parameters and domain structure. Shaded region represents the range of 100 best fit model results. Solid line is the mean. Also shown are the (U-Th)/He ages of zircon and apatite. Inset box shows the thermal history expanded to include coexisting biotite. Note that the biotite age is consistent with the projection of the slow cooling portion of the history.

equilibrate during the second isothermal increment, we relied on these results to extract kinetic parameters.

[31] Modeled thermal histories for these samples are also characterized by slow cooling during the Mesozoic and early Cenozoic (Figures 6d and 7d). Because these K-feldspars were more retentive of argon than the plateau margin samples, their modeled temperature-time paths extend to higher temperatures and older ages, permitting a direct comparison of the results with the biotite $^{40}Ar/^{39}Ar$ data for 97-4 and 97-6 (Figures 6dand 7d, respectively). In both cases, the biotite data are consistent with the K-feldspar cooling models.

4.2.3. Southern Longmen Shan. [32] Sample 93-1 was collected from the southern portion of the Baoxing massif, in the southern Longmen Shan region (Figure 2). Its release spectra show

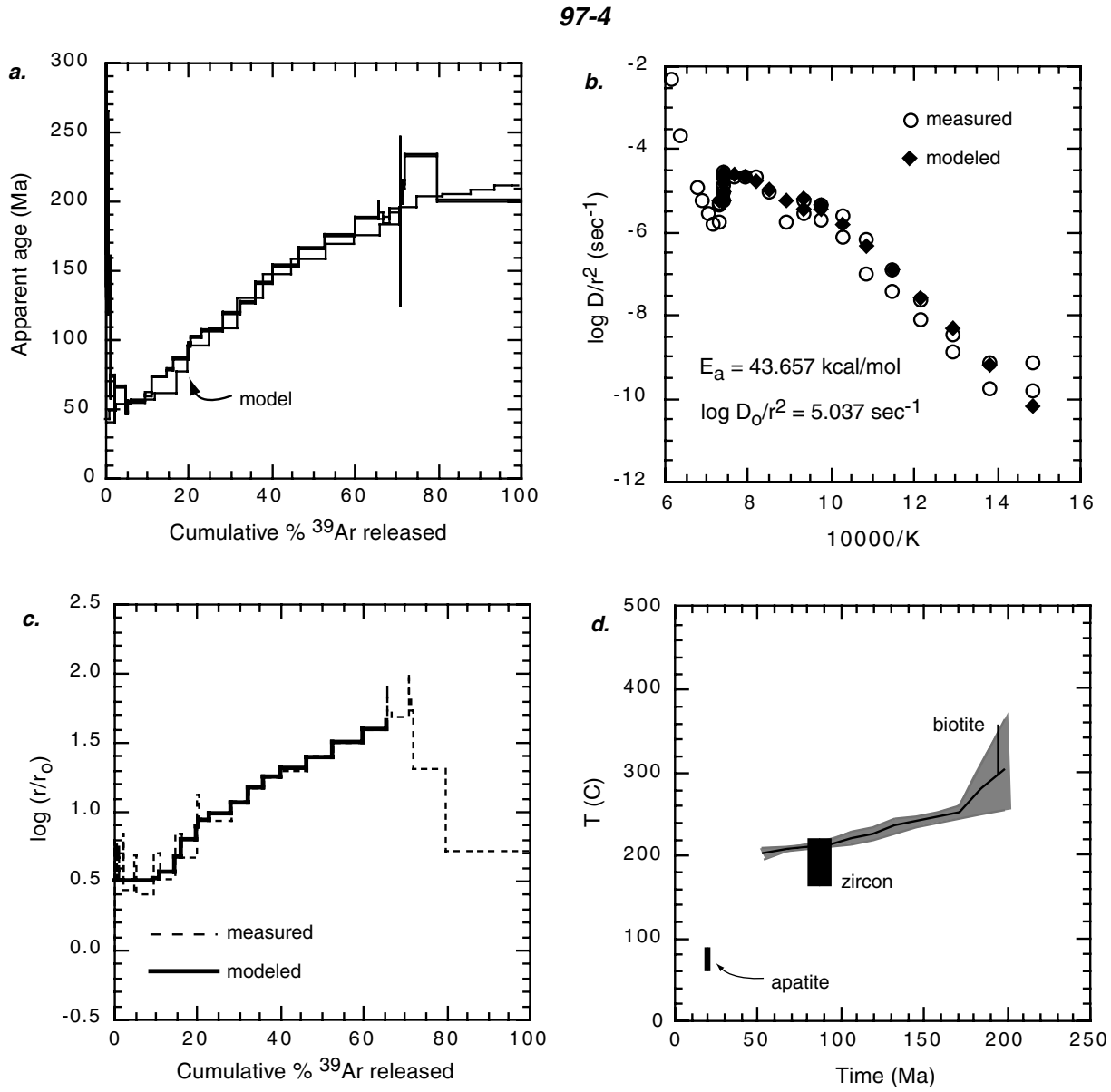

Figure 6. (a) $^{40}Ar/^{39}Ar$ release spectrum (open boxes) and mean of 100 modeled age spectra (solid line) for alkali feldspar collected from a granitoid pluton at ~2000 m, in the headwater reaches of the Hei Shui He. (b) Arrhenius plot of log D/r^2 versus reciprocal temperature. Arrhenius data are calculated assuming plane slab diffusion geometry from measured ^{39}Ar release during incremental heating experiment. (c) Plot of log (r/r_o) versus ^{39}Ar released (dashed line) and theoretical fit (solid line) from model. (d) Model thermal history for sample 97-4 obtained from inverse modeling of the kinetic parameters and domain structure. Shaded region represents the range of 100 best fit model results. Solid line is the mean. Also shown are the (U-Th)/He ages of coexisting apatite and zircon and the $^{40}Ar/^{39}Ar$ age of biotite.

evidence for considerable excess ^{40}Ar contamination of the low temperature steps and a remarkable monotonic increase in the apparent ages of higher temperature steps from ~65 Ma to ~550 Ma.

[33] MDD modeling of the thermal history of this spectrum suggests relatively slow cooling between ~350 Ma and ~100 Ma (Figure 8d). Beyond this range the model is poorly constrained. This result is surprising because independent evidence implies that the southern Longmen Shan had a complex tectonothermal history over much of the ~350–100 Ma interval. For example, the region was the locus of voluminous basaltic volcanism during the Permian (Emei flood basalt) and of severe shortening during the Mesozoic [*Chen et al.*, 1994a; *Burchfiel et al.*, 1995]. It may be that the assumption of monotonic cooling for the purpose of multidomain modeling is inappropriate over this time interval, and we unfortunately have no other geochronologic data that might corroborate the result. In any event, the absence of Cenozoic ages in the low-temperature portions of the release spectrum appear to indicate that

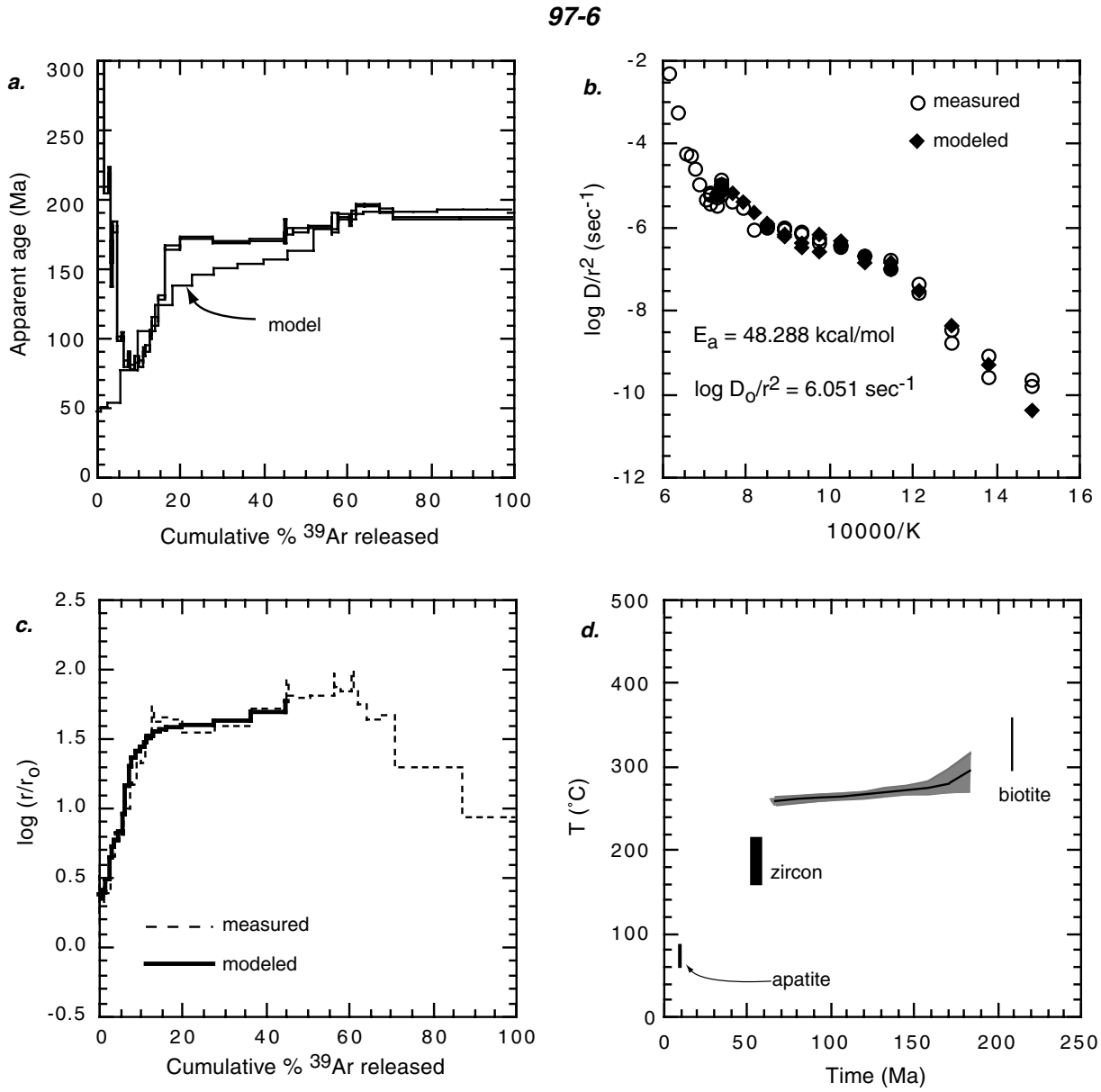

Figure 7. (a) $^{40}Ar/^{39}Ar$ release spectrum (open boxes) and mean of 100 modeled age spectra (solid line) for alkali feldspar collected from a granitoid pluton at ~4000 m, in the headwaters of the Hei Shui He. (b) Arrhenius plot of log D/r^2 versus reciprocal temperature. Arrhenius data are calculated assuming plane slab diffusion geometry from measured ^{39}Ar release during incremental heating experiment. (c) Plot of log (r/r_o) versus ^{39}Ar released (dashed line) and theoretical fit (solid line) from model. Note that the data for the last ~50% of the gas were released above the incongruent melting temperature for alkali feldspar and thus contain no volume diffusion information. (d) Model thermal history for sample 97-6 obtained from inverse modeling of the kinetic parameters and domain structure. Shaded region represents the range of 100 best fit model results. Solid line is the mean. Also shown are the ages of coexisting apatite, zircon ((U-Th)/He) and biotite ($^{40}Ar/^{39}Ar$).

the sample resided at relatively high levels in the crust prior to Cenozoic time.

4.3. (U-Th)/He Results

[34] (U-Th)/He thermochronology is a recently redeveloped technique that provides age information in the low-temperature range of thermochronologic systems [*Zeitler et al.*, 1987; *Lippolt et al.*, 1994; *Wolf et al.*, 1996; *House et al.*, 1997; *Warnock et al.*, 1997; *Wolf et al.*, 1997]. Helium diffusion in most fluorapatite appears to be a thermally activated process with a nominal closure temperature (for a cooling rate of 10°C/m.y.) of ~70°C [*Farley*, 2000]. Preliminary work on helium diffusion in zircon suggests that the closure temperature ($dT/dt$of 10°C/m.y.) is probably

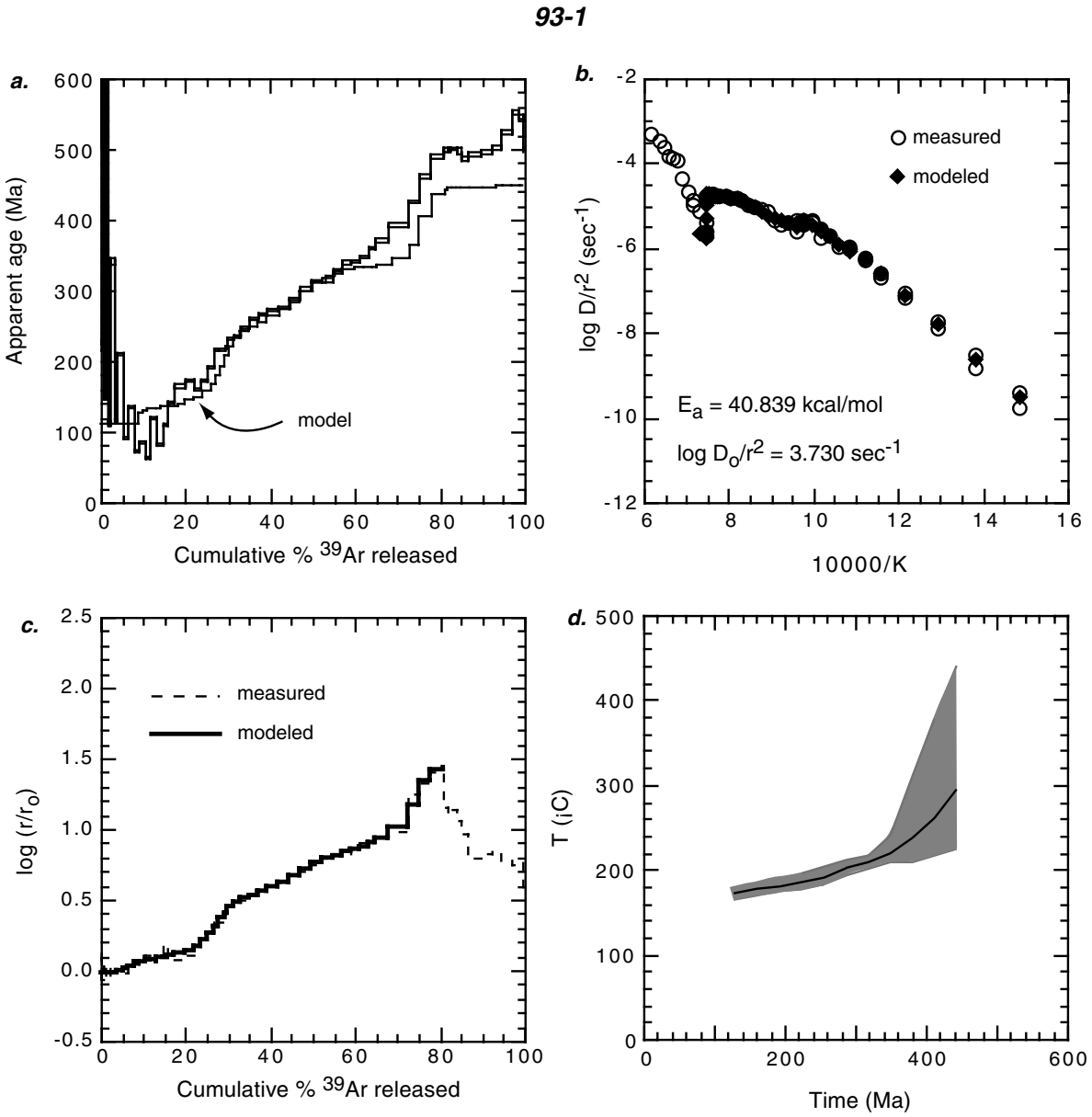

Figure 8. (a) $^{40}Ar/^{39}Ar$ release spectrum (open boxes) and mean of 100 modeled age spectra (solid line) for alkali feldspar collected from the Baoxing massif, southern Longmen shan. (b) Arrhenius plot of log D/r^2 versus reciprocal temperature. Arrhenius data are calculated assuming plane slab diffusion geometry from measured ^{39}Ar release during incremental heating experiment. (c) Plot of log (r/r_o) versus ^{39}Ar released (dashed line) and theoretical fit (solid line) from model. (d) Model thermal history for sample 93-1 obtained from inverse modeling of the kinetic parameters and domain structure. Solid lines represent the mean (solid) and bounds (shaded) of 100 best fit results. Dashed lines represent portions of the model thermal history outside the range of ages recorded in the feldspar.

between 180° and 200°C [*Reiners et al.*, 2002]. However, some aspects of zircon helium diffusion characteristics, possibly related to radiation damage, are not well understood at present; for the purposes of this work, we consider a possible closure temperature range of 160°–210°C. Details of the analytical procedures associated with age determination are presented in Appendix A. Data for apatite and zircon analyses from samples in this study are presented in Table 1; sample locations and associated ages are presented in Figure 2.

[35] Helium ages in both zircon and apatite cluster in two distinct populations that reflect the variations observed in the feldspar thermal models. Samples collected from the topographic margin of the plateau record systematically younger ages (late Miocene to Pliocene in both systems) than those from the plateau interior (Late Cretaceous/early Tertiary in zircon and mid-Miocene in apatite). Samples from the Pengguan massif (93-3 and 93-4, ~900 m elevation), along the margin of the plateau adjacent to the Sichuan Basin, yielded an age of 4.6 ± 0.3 Ma in apatite and 11.0 ±

Table 1. Analytical Data for (U-Th)/He Age Determinations From Apatite and Zircon in the Longmen Shan Region[a]

Sample	Sample Material	He, (ncc)/mg	U, ppm	Th, ppm	Ft[b]	Corrected Age (Ma)	Average Age (Ma)[c]
93-3	apatite	2.113	3.7	10.7	0.61	4.57	4.6 ± 0.7[d]
93-4	zircon	366.7	340.0	241.6	0.694	11.02	11.0 ± 0.9
97-2(a)	apatite	44.877	30.3	9.5	0.793	14.29	13.4 ± 0.8
97-2(b)	apatite	21.427	18.9	5.7	0.694	12.53	
97-4	apatite	19.937	10.7	12.0	0.609	19.92	19.9 ± 1.2
97-4	zircon	3085	353.8	50.0	0.801	86.8	86.8 ± 6.9
97-5	apatite	15.302	6.8	12.7	0.623	20.57	20.6 ± 1.2
97-6(a)	apatite	9.149	11.3	19.2	0.643	7.39	8.2 ± 0.5
97-6(b)	apatite	11.016	11.1	16.4	0.676	8.97	
97-6	zircon	2944	543.3	123.6	0.773	55.0	55.0 ± 4.4
97-14	apatite	4.331	14.6	20.1	0.578	3.19	3.2 ± 0.5[d]
94-14	zircon	304.3	689.5	188.8	0.733	4.69	4.7 ± 0.4

[a]See MAppendix A for analytical procedures.
[b]Ft is a geometrical correction for alpha ejection [*Farley et al.*, 1996].
[c]Average ages are mean ages of duplicate analyses (where appropriate). Uncertainties are based on reproducibility of laboratory standards and are taken as 6% (2σ) for apatite and 8% (2σ) for zircon (see Appendix A for details).
[d]For samples with low helium yields, we adopt a conservative 2σ uncertainty of 15%.

0.9 Ma in zircon. A sample from the eastern foot of the Min Shan (97-14, ∼1100 m elevation) yielded an apatite age of 3.2 ± 0.5 Ma and a zircon age of 4.7 ± 0.4 Ma. It is worth noting that sample 93-3 was collected in close proximity to two apatite fission track samples of *Arne et al.* [1997] and yields an age that is statistically indistinguishable from their results (see Figure 2).

[36] Samples collected from the plateau yielded apatite ages of 13.4 ± 0.8 Ma (97-2, ∼1800 m elevation), 19.9 ± 1.2 Ma (97-4, ∼2000 m elevation), 20.6 ± 1.2 Ma (97-5b, ∼4500 m elevation), and 8.2 ± 0.5 Ma (97-6, ∼4300 m elevation). Although these samples span ∼2 km of relief, there is little correlation between age and elevation. Given the limited number of samples and their geographic distribution, however, we can say little about the geometry and position of the partial retention zone for He over the time interval of interest [*Wolf et al.*, 1998]. An additional complication is introduced by the anomalously young age of one of the highest samples (97-6). At present, we cannot address whether there is substantial variation in apatite (U-Th)/He ages from the surface of the plateau [e.g., *House et al.*, 1998]. Zircon from two of these samples (97-4 and 97-6) yielded ages of 86.8 ± 6.9 and 55.0 ± 4.4, respectively. Thus the variation in cooling ages between the topographic margin of the plateau and the interior appears to be a robust feature of both the apatite and zircon (U-Th)/He data. Similar variations in apatite fission track ages were observed in the Longmen Shan [*Arne et al.*, 1997] and to the south, along the Xianshuihe fault [*Xu and Kamp*, 2000].

4.4. Comparison of Feldspar Thermal Models and (U-Th)/He Data

[37] One of the most striking results of this combined data set is the correspondence between the thermal histories derived from the feldspar MDD models and the (U-Th)/He data. In all samples where we have multiple systems whose ages overlap, the feldspar models are consistent with (U-Th)/He ages. This is particularly true of samples from the plateau margin (93-4 and 97-14), where the zircon and apatite ages tightly bracket the rapid increase in cooling rate inferred from the thermal models (Figures 4and 5). Thus we are encouraged that feldspar MDD models retain reliable geologic information about the thermal histories experienced by these samples.

4.5. Summary: Cooling History of the Longmen Shan Region

[38] Thermal histories inferred from the combination of $^{40}Ar/^{39}Ar$ thermochronometry on biotite, (U-Th)/He thermochronometry on apatite and zircon, and alkali feldspar MDD modeling provide a relatively complete picture of the low-temperature cooling history of rocks in the Longmen Shan region following Mesozoic tectonism. Despite differences in age and in structural setting, all samples are characterized by remarkably slow cooling (<1°C/m.y.) between the early Jurassic and the mid-Tertiary (Figure 9 and Table 2). However, samples from the topographic front of the plateau margin (93-4 and 97-14) record systematically younger zircon and apatite (U-Th)/He ages than samples from the plateau interior (97-4 and 97-6). These differences are captured by feldspar thermal models which record a pronounced increase in cooling rate in the late Miocene and early Pliocene at the plateau margin. The Cenozoic thermal history of samples from the plateau interior is somewhat less well defined; cooling rates appear to have increased (∼2°–4°C/m.y.) at some point between complete feldspar closure (∼50–70 Ma) and apatite ages (∼20–8 Ma). However, our data do not constrain when during this interval the increase took place. Plausible scenarios are discussed in section 7.1, but confident interpretation of thermal history of this region during the mid-Tertiary awaits additional data. Regardless, it is clear that samples from the plateau resided at or below the closure temperature for helium in apatite by the late Miocene/early Pliocene. In what follows, we explore the implications of these variations in the thermal history between the plateau margin and its interior for the degree and extent of late Cenozoic denudation.

5. Rates and Pattern of Denudation

[39] The inference of denudation rate from thermochronologic data is often complicated by time-dependent thermal regimes whose evolution depends on the advection of heat during denuda-

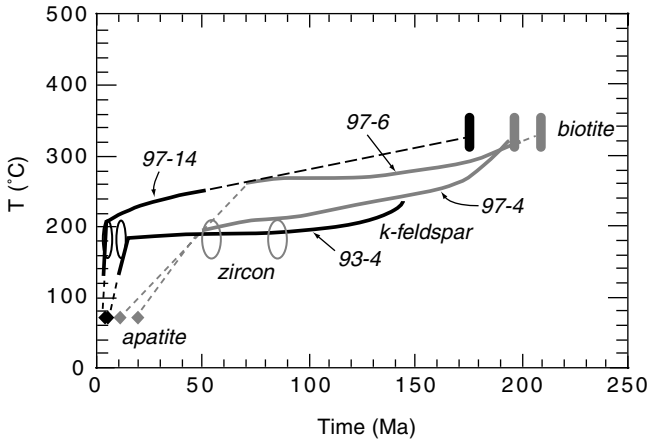

Figure 9. Composite thermal histories for samples from the Longmen Shan region. Biotite ages are represented by rectangles, apatite ages by diamonds, zircon ages by open ellipses, and K-feldspar model thermal histories are shown as solid lines. Dashed lines show the inferred cooling paths between data points. Samples from the present-day topographic margin (solid) and samples from the interior of the plateau (shaded) are shown. Regional slow cooling during the Mesozoic and early Cenozoic implies long-term thermal stability. Rapid cooling of samples at the margin of the plateau initiates in the late Miocene-early Pliocene and is inferred to record the onset of rapid denudation during Cenozoic development of the plateau.

tion [e.g., *Moore and England*, 2001]. However, the regional extent and remarkably slow rate of cooling between the mid-Mesozoic and the Cenozoic suggests the establishment and persistence of a stable thermal regime following Mesozoic tectonism. If we make the reasonable assumption that isotherms during this time were subhorizontal and that cooling reflects the motion of rocks through this thermal structure because of erosional denudation, we can translate cooling rates into estimates of denudation rate. For geotherms typical of stable continental regions (15°–25°/km), cooling rates of <1°/m.y. imply that denudation rates must have been extremely slow (<0.1 mm/yr). These rates would have persisted over much of the region until at least the early Eocene and, importantly, over the position of the present margin until the latest Miocene (Table 2 and Figure 9).

[40] Rapid late Cenozoic cooling observed in samples from the margin of the plateau (Table 2) implies that denudation rates increased substantially in the late Miocene. However, an estimate of their magnitude is complicated by the advection of heat during rapid denudation [*Mancktelow and Grasemann*, 1997]. We can, nevertheless, estimate the depth of the sample prior to the onset of rapid cooling and obtain a mean denudation rate over the period of the rapid cooling event. Both samples from the topographic margin record the onset of rapid cooling at ~200°C, implying ~8–10 km of denudation during the late Cenozoic (for nominal geotherms). For sample 93-4 (Longmen Shan) this translates into mean denudation rates on the order of 1 mm/yr, while for sample 97-14 (Min Shan), denudation rates appear to have been ~1–2 mm/yr.

[41] In contrast, samples from the Songpan-Garze terrane appear to record lesser degrees of late Cenozoic denudation. The youngest ages recorded by feldspars range from 50–70 Ma and are consistent with zircon (U-Th)/He ages of 55–85 Ma. Together, these indicate that rocks now exposed at and near the plateau surface had cooled below ~200°C by the early Tertiary. Furthermore, the presence of (U-Th)/He apatite ages between 8 and 20 Ma indicates that Miocene-Recent denudation on the plateau has been limited to a few kilometers. Thus the data suggest that late

Table 2. Cooling Rates Inferred From Thermochronologic Analyses in the Longmen Shan Region[a]

Location	Age Range, Ma	Temperature	Cooling Rate, deg/m.y.	Mineral System
Min Shan (97-14)	170–6	350°–200°C	~1°	biotite/feldspar
	5–3	200°–75°C	50°–60°	zircon/apatite
	3–0	75°–20°C	~20°	
Longmen Shan (93-3, 93-4)	150–11	240°–190°C	~0.5°	feldspar
	11–4	190°–75°C	15°– 20°	zircon/apatite
	4–0	75°–20°C	~15°	
Songpan-Garze (97-4)	195–50	350°–190°C	~1°	biotite/feldspar/zircon
	50–20	190°–75°C	3°–4°	feldspar/apatite
	20–0	75°–20°C	~3°	
Songpan-Garze (97-6)	210–70	350°–250°C	~ 0.6°	biotite/feldspar
	55–8	180°–75°C	2°–3°	zircon/apatite
	8–0	75°–20°C	~7°	zircon/apatite

[a]Nominal closure temperatures for biotite, zircon, and apatite are taken as ~350°C [*Grove and Harrison*, 1996], ~180°–200°C [*Reiners et al.*, 2002], and ~75°C [*Farley*, 2000], respectively.

Cenozoic denudation has been heterogeneous across the eastern margin of the plateau adjacent to the Sichuan Basin, with high rates focused in a narrow zone along the present topographic front. These results are broadly consistent with the distribution of denudation inferred from apatite and zircon fission track ages in the Longmen Shan region [*Arne et al.*, 1997] and along the margin of the plateau south and west of the Xianshuihe fault [*Xu and Kamp*, 2000].

[42] The increase in cooling rate experienced by samples from the plateau interior during the early to middle Tertiary (~50–20 Ma; Table 2 and Figure 9) suggests a concomitant increase in denudation rate. As noted in section 4.5, the form of the cooling path, and thus, the timing of the increase in denudation rate, during this interval is not constrained by our data, and we can only estimate mean denudation rates during this interval using a linear extrapolation between data points. Mean denudation rates appear to have been on the order of 0.1–0.2 mm/yr (for nominal geotherms). Whether this apparent increase in denudation rate is tectonically significant will be considered in section 7.1.

6. Onset of Rapid Denudation

[43] The apparent focusing of late Cenozoic denudation along the present topographic margin of the plateau and subsequent exhumation of rocks from upper midcrustal depths allows us to place an upper bound on the onset of rapid cooling. Adjacent to the Sichuan Basin the close correspondence between a zircon (U-Th)/He age of ~11 Ma and the transition from slow to rapid cooling (11–12 Ma) in the feldspar thermal model suggest that this sample still resided at temperatures ~200°C at circa 11 Ma. The onset of rapid cooling is therefore bracketed between 11 Ma and 4.5 Ma (the age of the corresponding apatite). Likewise, in the Min Shan, the onset of rapid cooling in the feldspar model (5–6 Ma) corresponds almost exactly with the zircon age (~5 Ma), restricting the onset of rapid cooling to between 5 and 3 Ma.

[44] Evaluating whether or not these transitions also represent the onset of rapid denudation is problematic. For example, the advection of heat that accompanies an increase in denudation rate imparts a phase lag between the onset of rapid denudation and rapid cooling that complicates a direct interpretation of the onset of rapid cooling [*House and Hodges*, 1994; *Stuwe et al.*, 1994; *Mancktelow and Grasemann*, 1997]. As packages of rock are translated toward the surface along with isotherms, cooling is delayed until they pass through compressed isotherms near the surface [*Moore and England*, 2001]. However, simple modeling of the advective/conductive transfer of heat in response to rapid denudation in extensional settings [*Ruppel et al.*, 1988] suggests that this lag time is relatively short (1–2 m.y.) in the upper regions of the crust. Therefore our estimates of the onset of rapid cooling in the Longmen Shan are probably a close proxy for the onset of rapid denudation. We estimate that the onset of rapid denudation probably occurred no earlier than 12–13 Ma in the Longmen Shan and no earlier than 6–7 Ma in the Min Shan. It is important to note that these are maximum estimates; denudation could have begun as recently as 5–6 Ma in the Longmen Shan and as recently as 4–5 Ma in the Min Shan.

[45] The difference in cooling ages and inferred denudation rates between the Longmen Shan and the Min Shan may be an indication of diachroneity in the onset of deformation between different regions along the modern plateau margin. However, given that cooling could have begun as recently as 5–6 Ma in the Longmen Shan, we cannot say with confidence whether this apparent difference reflects true variability in the timing of plateau formation. A definitive test of this possibility awaits further sampling.

7. Tectonic Implications

7.1. Timing of Uplift in Eastern Tibet

[46] The timing and rates of denudation across the eastern margin of the Tibetan Plateau have important implications for the development of topography in this region. As discussed in section 2, regional topographic gradients between the plateau and the Sichuan Basin are among the highest anywhere on the continents. Given the structural position of the samples at the foot of this topographic escarpment, it is unlikely that the slow denudation rates inferred prior to the late Miocene/early Pliocene could have been maintained in the presence of such extreme topographic gradients. This scenario requires climatic conditions approaching those in present-day Antarctica [*Brook et al.*, 1995], and is clearly not appropriate for central Asia during the Miocene. Indeed, present-day incision rates along rivers draining this margin range from 1 to 2 mm/yr [*Kirby and Whipple*, 2000], attesting to the erosive power of streams along the eastern front of the escarpment. Thus we interpret the pronounced late Miocene increase in cooling rates as marking the initial development of regionally significant topographic gradients at the present plateau margin, presumably in response to crustal thickening.

[47] Determining the Tertiary denudation history in the headwater regions of the river valleys west of the Longmen Shan is complicated by the incomplete resolution of our data. As noted in section 4.5, our data do not discriminate between a period of slightly enhanced denudation and cooling starting in the early Tertiary and a prolonged period of slow cooling followed by an rapid increase in the middle to late Miocene. We prefer the latter scenario for several reasons. First, *Arne et al.* [1997] collected an age-elevation transect of apatite fission track samples that is located midway between the plateau margin and the interior. Apatite fission track ages are invariant over ~1500 m and range from ~4–7 Ma (Figure 2), implying relatively rapid cooling during the late Miocene and early Pliocene. As there are no major structural discontinuities between these samples and our plateau samples, this site probably represents a similar structural level. Second, a regional study of apatite fission track ages along the Xianshuihe fault [*Xu and Kamp*, 2000], south and west of the Longmen Shan region, concluded that much of the region was cooling slowly between circa 130 Ma and circa 22 Ma. Finally, a recent study of apatite (U-Th)/He ages in the same region [*Clark et al.*, 2000] is consistent with slow cooling (~1°C/m.y.) from 25-9 Ma. From a regional perspective it appears that much of eastern Tibet was characterized by relatively slow cooling during the early and mid-Tertiary. While denudation rates may have increased (~0.1–0.2 mm/yr) on the plateau west of the Longmen Shan sometime during early Tertiary, we believe that it is more likely that rates remained slow until the Miocene.

[48] Slow denudation during the early and mid-Tertiary, however, does not preclude the existence of substantial elevation in the region. The region west of the plateau margin was a source for sediment in the Sichuan Basin from Jurassic times [*Burchfiel et al.*,

1995] and may have been a residual highland from the Mesozoic orogeny. Although we find it unlikely that such low denudation rates (<0.1 mm/yr) could be maintained on steep regional topographic gradients, it is possible that a gently sloping, low-relief upland existed in the region prior to Cenozoic tectonism. Thus we can conclude little at this time about the absolute magnitude of elevation changes as a result of the development of the Tibetan Plateau in this region.

7.2. Landscape Evolution Along the Eastern Margin

[49] The thermal histories presented here have important implications for the long-term morphologic evolution of the eastern Tibetan Plateau adjacent to the Sichuan Basin. In particular, our data place preliminary bounds on (1) the "age" of the present surface of the plateau and (2) the evolution of the modern relief along the escarpment. As described in section 2, large regions of the eastern plateau comprise a low-relief surface cut on vertically foliated Triassic flysch. Although this surface (and any "erosion surface") is a dynamic landform, currently evolving as an erosional and depositional feature, one can define three useful temporal characteristics of such a surface: (1) the time at which the surface was reduced to low relief, (2) the duration of such relief, characterized by slow erosion rates, and (3) the time at which the surface began to be significantly dissected. While our data are far from comprehensive, the thermal histories of samples from the surface (97-6) and 2 km below it (97-4) suggest that the low relief atop the eastern plateau today may have developed in the Mesozoic and been sustained since then by relatively slow uniform denudation. Subsequent dissection of this surface in response to the development of regional topographic gradients between the plateau and the Sichuan Basin apparently initiated in the late Miocene or early Pliocene, and most of the local relief along the margin (which now exceeds 3 km) probably developed since that time.

7.3. Timing of Normal Faulting in the Longmen Shan

[50] Our results from the Pengguan Massif, adjacent to the Sichuan Basin, place additional constraints on the timing of normal faults developed within the Longmen Shan thrust belt. The massif is an elongate NE trending body of Precambrian gneisses and granitoids and is bounded on the NW by a series of low-grade mylonite zones with top to the NW sense of displacement [*Burchfiel et al.*, 1995]. Although it is possible that displacement on these fault systems is responsible for some of the rapid cooling observed since ~11 Ma, we see no evidence for a 25–30 Ma event as suggested by *Hames and Burchfiel* [1993]. Indeed, throughout the Longmen Shan, our data suggest that the early and mid-Miocene was characterized by regionally uniform slow cooling. Thus, if the faults have Cenozoic displacement, it appears to be restricted to the late Miocene-Pliocene. We note that Cenozoic displacement on these faults provides a mechanism for exhumation without large amounts of net shortening across the margin. However, the exact timing of displacement on these normal fault systems remains an important problem in this region.

7.4. Processes of Plateau Formation

[51] The apparent absence of large magnitude Cenozoic shortening of the upper crust in eastern Tibet [*Burchfiel et al.*, 1995; *Wang et al.*, 1998; *Kirby et al.*, 2000] suggests that crustal thickening may have been accomplished by ductile flow in a weak lower crust [*Royden*, 1996; *Royden et al.*, 1997]. A recent analysis of the regional topography in eastern Tibet [*Clark and Royden*, 2000] suggests that the morphology of the plateau margins may be a consequence of the strength of the foreland region; adjacent to the Sichuan Basin the margin is steep because weak lower crust ponds against a strong foreland region, while in southeastern Tibet a weak foreland allows the development of a diffuse topographic transition between the plateau and the foreland. Our results bear on two aspects of this model: (1) the nature and degree of upper crustal deformation and (2) the lateral growth of the plateau.

[52] The amount and timing of Cenozoic shortening within this region of eastern Tibet have been the subject of some debate. Although most workers in the region acknowledge that there has been Cenozoic displacement on a number of the faults in the region [*Chen et al.*, 1994b; *Dirks et al.*, 1994; *Burchfiel et al.*, 1995; *Arne et al.*, 1997; *Kirby et al.*, 2000], the magnitude and rates are uncertain [cf. *Avouac and Tapponnier*, 1993; *Burchfiel et al.*, 1995]. The sharp contrast in cooling histories between rocks along the plateau margin and those in the foreland implies that there has been ~8–10 km of slip since the late Miocene along the frontal fault system adjacent to the Sichuan Basin. This displacement could be easily accommodated over the past 5–10 m.y. by mean slip rates of ~1–2 mm/yr. Such rates are consistent with the observed geodetic measurements that restrict modern shortening to <2–3 mm/yr [e.g., *Chen et al.*, 2000] and with the observation of limited Cenozoic shortening in the southern Longmen Shan [*Burchfiel et al.*, 1995].

[53] A similar contrast in cooling histories across the eastern front of the Min Shan implies that a similar amount of exhumation must be accommodated along the eastern range front. Our results, in conjunction with Cretaceous apatite fission track ages obtained by *Arne et al.* [1997], indicate that substantial late Cenozoic denudation in the Min Shan region was confined to a narrow (<40 km) corridor along the eastern flank of the range (see Figure 2). Differential exhumation was probably facilitated by displacement on the Huya fault and associated structures (Figure 2).

[54] A number of geodynamic models of plateau development [*England and Houseman*, 1986], including those invoking lower-crustal flow [*Royden et al.*, 1997], suggest that the plateau grew laterally with time. If the plateau has been growing east and northeast by the evacuation of lower crust from beneath the plateau, our results suggest that it did not begin to abut the Sichuan Basin until at least ~11–12 Ma (perhaps as young as 5–6 Ma) and contradict the recent suggestion that the present configuration of the plateau margins was established by circa 20 Ma [*Xu and Kamp*, 2000].

[55] The slight increase in Tertiary cooling rates observed in the samples from the interior of the plateau could reflect the development of a migrating wedge of topography built as lower crust was evacuated from beneath central Tibet [e.g., *Clark and Royden*, 2000]. It is important to note, however, that there is no indication in our data of a steep former topographic margin, subject to deep erosion. Rather, the relatively slow cooling rates of samples now on the plateau (2°–4°C/m.y.; Table 2) imply that it would have had a relatively gentle regional slope, perhaps analogous to the present situation in southeastern Tibet. A definitive test of this hypothesis, however, awaits further sampling.

[56] Finally, the distribution of Cenozoic denudation across the eastern margin of the plateau has important implications for the coupling between surficial and tectonic processes along the margin.

Our results suggest that since the late Miocene/early Pliocene, denudation has been heterogeneous across the plateau margin. In both the Longmen Shan and Min Shan regions the zone of deepest exhumation corresponds to the present-day topographic front of the plateau and to a zone of high gradients along modern rivers [*Kirby and Whipple*, 2000; *Kirby*, 2001]. This spatial correlation of long-term exhumation of midcrustal rocks and steep river gradients may reflect the erosional enhancement of mass flux along this margin [e.g., *Beaumont et al.*, 1992; *Willett*, 1999], and it raises the possibility that the steep topography adjacent to the Sichuan Basin is, in part, a response to high erosion rates along the margin.

8. Conclusions

[57] Thermal histories derived from integrated $^{40}Ar/^{39}Ar$ and (U-Th)/He dating of samples along the eastern margin of the Tibetan Plateau place important constraints on the timing of development of high topography adjacent to the Sichuan Basin. The data suggest that this region of the plateau was characterized by slow cooling (~1°C/m.y.) and a stable thermal regime following Mesozoic tectonism and pluton emplacement. These cooling rates apparently persisted in samples from the topographic front of the plateau until the late Miocene. We infer that mean erosion rates during this time period were concomitantly slow (<0.1 mm/yr for nominal geothermal gradients between 10°C/km and 30°C/km). Cooling rates in the interior of the plateau apparently increased (~2°–4°C/m.y.) during the early to middle Tertiary, although the timing and tectonic significance of this increase remain uncertain.

[58] Rapid cooling observed in samples from the present-day margin of the plateau began between 11 and 5 Ma adjacent to the Sichuan Basin and between 5 and 3 Ma in the Min Shan. This cooling is interpreted to reflect rapid erosion focused along the developing topographic margin. The relatively deep exhumation of rocks (~8–10 km) along this margin provides a unique record of the onset of rapid cooling as recorded in $^{40}Ar/^{39}Ar$ and (U-Th)/He isotopic systems. Thus the present margin of the plateau does not appear to have been established in this region prior to the late Miocene or early Pliocene.

[59] We caution, however, that this estimate does not apply to the plateau as a whole. Plateau uplift, if driven by crustal thickening, may be quite heterogeneous in space and time. Our data hint at the possibility that the plateau may have grown laterally with time, perhaps as a diffuse topographic wedge. In addition, there may have been significant variability (up to ~5 Ma) in the onset of rapid cooling between segments of the margin adjacent to and north of the Sichuan Basin. Only when we develop similar estimates of the timing of plateau uplift along many of its other margins, former and present, will we be able to comprehensively assess the timing and mechanisms of plateau formation.

Appendix A: Analytical Methods

A1. $^{40}Ar/^{39}Ar$ Techniques

[60] Pure mineral separates were prepared from crushed material using standard heavy liquid and magnetic methods. In all cases, material was handpicked to ensure sample homogeneity (>99%). Mineral separates were washed in distilled water, acetone, and ethanol prior to packaging in Al foil for irradiation. Individual packets were loaded in aluminum disks, shielded with Cd foil, and irradiated in the core position of the research reactor at McMaster University, Ontario, Canada.

[61] K and Ca production factors during irradiation were established by analyzing reagent grade K_2SO_4 and CaF_2 included in each package. Isotopic correction factors are as follows: $^{36}Ca/^{37}Ca$, 3.38×10^{-4}; $^{38}Ca/^{37}Ca$, 2.04×10^{-4}; $^{39}Ca/^{37}Ca$, 9.54×10^{-4}; $^{36}Cl/^{38}Cl$, 1481; $^{37}K/^{39}K$, 2.07×10^{-4}; $^{38}K/^{39}K$, 1.16×10^{-2}; $^{40}K/^{39}K$, 5.00×10^{-3}. Fast neutron flux was monitored using Fish Canyon sanidine (27.95 Ma) [*Cebula et al.*, 1986] and McClure Mountain (MMhb-1) hornblende (520.4 Ma) [*Samson and Alexander*, 1987]. Monitors were analyzed by total fusion of 1–5 crystals with an Ar-ion laser. Flux gradients are typically negligible within a disk, but the irradiation parameter, *J*, may vary by up to 2% along the length of a package [*Hodges et al.*, 1994]. We assigned the mean *J*calculated for a disk to all samples in that disk. We assume a conservative 2% uncertainty in *J* (at 2σ) for all samples in order to account for potential uncertainties in interpolation of *J* between monitor positions and in potential heterogeneities in monitor materials. Ages stated in the text and figures include this propagated uncertainty.

[62] Resistance furnace gas extraction was accomplished using a double-vacuum assembly in the Massachusetts Institute of Technology (MIT) Noble Gas Laboratories. Details of the extraction line are given by *Hodges et al.* [1994]. Temperatures were continuously monitored using a Re-W thermocouple; this system provides ~5°C control on temperature over the course of a heating increment. All samples were allowed to equilibrate with the ambient furnace temperature (250°C) for 5 min prior to analysis.

[63] Operational blanks for the resistance furnace extraction line are dominated by the furnace and are strongly temperature dependent. Furnace system blanks were measured as a function of temperature prior to sample analysis. Blank corrections were generally small; signal sizes were typically 2 to 3 orders of magnitude larger than the furnace system blank.

[64] After corrections were made for interfering isotopes, mass discrimination, and blank, $^{39}Ar/^{40}Ar$ data were analyzed in a variety of ways (see supporting data Table A1). The model age for each increment of gas extraction was calculated assuming an initial $^{40}Ar/^{36}Ar$ value of 295.5 and is assigned a 2σ uncertainty that reflects propagated errors in all correction factors and the *J* parameter. Release spectra illustrate model ages for incremental heating analyses as a function of the amount of $^{39}Ar_K$ in each step. Age plateaus determined from the incremental release spectra are defined as the error-weighted mean age of contiguous steps that define 50% or more of the total $^{39}Ar_K$ released, and they are statistically indistinguishable at the 2σ confidence level, exclusive of uncertainty in the *J* value. For the biotites in this study, none of the spectra define plateaus, and we use a weighted mean of selected contiguous steps as our best estimate of the bulk closure age of the sample. All uncertainties associated with the ages are reported at the 2σ level and include the uncertainty in the *J* factor but not uncertainties in the ages of the flux monitors.

[65] For the K-feldspar analyses, the heating schedule was varied in order to facilitate retrieval of kinetic information for each sample [*Lovera et al.*, 1991]. Heating schedules are presented along with $^{40}Ar/^{39}Ar$ data in supporting data Table A1. Activation

energies for the samples were obtained by fitting an unweighted linear regression to the initial, low-temperature diffusion data on Arrhenius diagrams. Domain size distributions were modeled from fits to the ^{39}Ar release data via $\log(r/r_o)$ plots [*Lovera et al.*, 1989; *Lovera et al.*, 1991; *Lovera*, 1992]. The model does not consider gas evolved above the temperature for incongruent melting of K-feldspar (~1150°C). For our samples we were typically able to model between 60 and 80% of the gas.

[66] Excess argon is often present in the first few percent of gas released and may obscure age information in the low-temperature portion of the experiment [*Harrison et al.*, 1993]. Recent experiments have shown that in many cases this excess argon is associated with the decrepitation of Cl-rich fluid inclusions [*Harrison et al.*, 1993, 1994]. In order to facilitate retrieval and interpretation of age information from the early portion of the gas release we subjected all samples to duplicate isothermal heating. In all cases, the first step at a given temperature increment yielded anomalously old ages, while the second step typically yielded younger ages, presumably permitting us to see through the effects of Cl-related excess argon and to obtain a geologically meaningful age. We are thus able to model the thermal history of the samples to fairly low temperature (in some cases as low as ~120°C).

[67] Once the domain structure and diffusion parameters are obtained, their thermal histories were explored using an automated inversion model [*Zeitler*, 1993]. The automated inversion model is based on the controlled random search algorithm (CRS), previously applied to modeling fission track data [*Willett*, 1997]. The CRS algorithm is used to find thermal histories, that when fed into a finite difference diffusion model, produce model age spectra (typically a set of 100) that match the observed spectrum derived from laboratory incremental heating. In describing the cooling history of our samples we used the mean temperature history for the 100 histories. In the advent of an episode of reheating, a unique solution for the thermal history is not possible. In contrast, solutions allowing only monotonic cooling tend to cluster tightly within the closure window for argon diffusion in the K-feldspar.

A2. (U-Th)/He Techniques

[68] Apatite was separated from crushed samples using standard magnetic and heavy liquid techniques at MIT. Mineral separates were hand picked to ensure sample homogeneity; apatites were selected on the basis of morphology, size, and the absence of visible defects and inclusions (helium associated with U- and Th-bearing silicate inclusions can produce anomalously old ages [*House et al.*, 1997; *Spotila et al.*, 1998]). Samples typically consisted of 10–20 crystals of apatite between 60 and 90 μm in diameter. Helium was degassed in a high-vacuum furnace and measured on a quadrupole mass spectrometer in the Noble Gas Laboratory of the California Institute of Technology (see *Wolf et al.* [1996] for details of the extraction line). Analytical precision is typically 6–8% (2σ), based on reproducibility of intralaboratory standards [*Wolf*, 1997]. Following *Farley et al.* [1996], measured He concentrations were corrected for alpha ejection. This was accomplished using a geometric factor, F_T, derived from the size and shape of crystals in each sample [*Farley et al.*, 1996]. F_T values ranged from 0.58 to 0.79. Estimated uncertainty in this parameter is ~4–6% (2σ), based on repeat measurements [*Spotila et al.*, 1998]. After helium extraction, samples were dissolved in HNO_3 and measured for U and Th contents by isotope dilution on an inductively coupled plasma mass spectrometer (ICP-MS) at California Institute of Technology (Caltech). Typical analytical precision is ~2% [*Spotila et al.*, 1998]. Together, these individual uncertainties propagate to yield a 2σ uncertainty of ±10% for individual ages [*Spotila et al.*, 1998]. On the basis of replicate analyses we adopt uncertainties (2σ) for our samples of 6% (Table 1). However, for samples with low helium yield (97-14 and 94-3) we adopt uncertainties of 15% (2σ).

[69] Zircon ages were measured in the WSU (U-Th)/He dating lab. Helium extraction was performed using a laser heating method adapted for zircons and similar to that of *House et al.* [2000]. For each sample, three crystals were picked from heavy mineral separates and loaded into ~1 mm Mo foil envelopes. Mo foils were heated in a Cu sample planchet under high vacuum by a ~10 W, 1 mm diameter, CO_2 laser beam, projected through a ZnS window. Each aliquot was heated to bright incandescence (estimated temperature ~1500°–1700°C) for ~5–8 min. ^{4}He blanks measured on empty foil envelopes by this method were typically <0.02 ncc STP ^{4}He. ^{4}He was measured by ^{3}He isotope dilution, cryogenic purification, and quadropole mass spectrometry, similar to the procedure at Caltech; these measurements have an estimated analytical uncertainty of ~1%. Following helium measurements, crystals were retrieved from foil and spiked with ^{229}Th and ^{233}U. Crystals were dissolved in a two-step procedure involving 3 days in HF-HNO_3 at 200°C, followed by 1 day in HCl at 200°C. U and Th measurements were made by isotope dilution using an HP4500-Plus quadropole mass spectrometer. U and Th measurements have an estimated analytical uncertainty of 1–2%. Alpha ejection effects were modeled using the method of *Farley et al.* [1996], modified for zircon morphology, density, and stopping distances. On the basis of replicate analyses of Fish Canyon Tuff and other intralab zircon standards during the period in which these samples were run, we estimate an analytical uncertainty of 8% (2σ).

[70] **Acknowledgments.** Our work in eastern Tibet has been supported by the NSF Continental Dynamics program (EAR-9614970 and EAR-9725723). Reviews by Mihai Ducea, Dave Foster, Brad Hacker, and Brian Wernicke significantly improved the manuscript. We wish to acknowledge preliminary (U-Th)/He and fission track analyses by Martha House (Caltech) and Shari Kelly (NMT) which, although not included here, were instrumental in helping us design a sampling strategy. We also thank Clark Burchfiel, Marin Clark, and Wiki Royden for lively discussions.

References

Armijo, R., P. Tapponnier, J. L. Mercier, and T. Han, Quaternary extension in southern Tibet: Field observations and tectonic implications, *J. Geophys. Res.*, *91*, 13,803–13,872, 1986.

Arnaud, N. O., M. Brunet, J. M. Cantagrel, and P. Tapponnier, High cooling and denudation rates at Kongur Shan, Eastern Pamir (Xinjiang, China) revealed by ^{40}Ar/^{39}Ar alkali feldspar thermochronology, *Tectonics*, *12*, 1335–1346, 1993.

Arne, D., B. Worley, C. Wilson, S. Chen, D. Foster, Z. Luo, S. Liu, and P. Dirks, Differential exhumation in response to episodic thrusting along the eastern margin of the Tibetan Plateau, *Tectonophysics*, *280*, 239–256, 1997.

Avouac, J. P., and P. Tapponnier, Kinematic model of active deformation in Central Asia, *Geophys. Res. Lett.*, *20*, 895–898, 1993.

Beaumont, C., P. Fullsack, and J. Hamilton, Erosional control of active compressional orogens, in *Thrust Tectonics*, edited by K. R., McClay, pp. 1–18, Chapman and Hall, New York, 1992.

Bohlen, S. R., A. Montana, and D. M. Kerrick, Precise determinations of the equilibria kyanite = sillimanite and kyanite = andalusite and a revised triple point for Al_2SiO_5 polymorphs, *Am. Mineral.*, *76*, 677–680, 1991.

Brook, E. J., E. T. Brown, M. D. Kurz, R. P. Ackert, G. M. Raisbeck, and F. Yiou, Constraints on age, erosion, and uplift of Neogene glacial deposits in the Transantarctic Mountains determined from in situ cosmogenic ^{10}Be and ^{26}Al, *Geology*, *23*, 1063–1066, 1995.

Burchfiel, B. C., Z. Chen, Y. Liu, and L. H. Royden, Tectonics of the Longmen Shan and adjacent regions, *Int. Geol. Rev.*, *37*, 661–735, 1995.

Cebula, G. T., M. J. Kunk, H. H. Mehnert, C. W. Naeser, J. D. Obradovitch, and J. F. Sutter, The Fish Canyon Tuff, a potential standard for the ^{40}Ar–^{39}Ar Ar and fission-track methods, *Terra Cognita*, *6*, 139–140, 1986.

Chen, S. F., and C. J. L. Wilson, Emplacement of the Longmen Shan Thrust-Nappe Belt along the eastern margin of the Tibetan Plateau, *J. Struct. Geol.*, *18*, 413–430, 1996.

Chen, S., C. J. L. Wilson, Z. Luo, and Q. Deng, The evolution of the western Sichuan foreland basin, southwestern China, *J. Southeast Asian Earth Sci.*, *10*, 159–168, 1994a.

Chen, S. F., C. J. L. Wilson, Q. D. Deng, X. L. Zhao, and Z. L. Luo, Active faulting and block movement associated with large earthquakes in the Min Shan and Longmen mountains, northeastern Tibetan Plateau, *J. Geophys. Res.*, *99*, 24,025–24,038, 1994b.

Chen, Z., and X. Chen, *On the Tectonic Evolution of the Western Margin of the Yangzi Block*, 172 pp., Chengdu Inst. of Geol. and Min. Res., Chengdu, China, 1987.

Chen, Z., B. C. Burchfiel, Y. Liu, R. W. King, L. H. Royden, W. Tang, E. Wang, J. Zhao, and X. Zhang, GPS measurements from eastern Tibet and their implications for India/Eurasia intracontinental deformation, *J. Geophys. Res.*, *105*, 16,215–16,227, 2000.

Chung, S., C. Lo, T. Lee, Y. Zhang, Y. Xie, X. Li, K. Wang, and P. Wang, Diachronous uplift of the Tibetan plateau starting 40 Myr ago, *Nature*, *394*, 769–773, 1998.

Clark, M. K., and L. H. Royden, Topographic ooze: Building the eastern margin of Tibet by lower crustal flow, *Geology*, *28*, 703–706, 2000.

Clark, M. K., M. House, L. H. Royden, B. C. Burchfiel, X. Zhang, W. Tang, and Z. Chen, River incision and tectonic uplift in eastern Tibet from low-temperature apatite U-Th/He thermochronology, *Eos Trans. AGU*, *81*(48), Fall Meet. Suppl., Abstract T52F-02, 2000.

Coleman, M., and K. Hodges, Evidence for Tibetan plateau uplift before 14 Myr ago from a new minimum age for east-west extension, *Nature*, *374*, 49–52, 1995.

Dirks, P., C. J. L. Wilson, S. Chen, Z. Lou, and S. Liu, Tectonic evolution of the NE margin of the Tibetan Plateau: Evidence from the central Longmen Mountains, Sichuan Province, China, *J. Southeast Asian Earth Sci.*, *9*, 181–192, 1994.

England, P., and G. Houseman, Finite strain calculations of continental deformation, 2, Comparison with the India-Asia collision zone, *J. Geophys. Res.*, *91*, 3664–3676, 1986.

England, P. C., and G. A. Houseman, The mechanics of the Tibetan Plateau, in *The Geological Evolution of Tibet*, vol. 326 A, edited by C. Chang, et al., pp. 301–320, Philos. Trans. of the R. Soc. of London, 1988.

England, P., and P. Molnar, Surface uplift, uplift of rocks, and exhumation of rocks, *Geology*, *18*, 1173–1177, 1990.

Farley, K. A., Helium diffusion from apatite: General behavior as illustrated by Durango fluorapatite, *J. Geophys. Res.*, *105*, 2903–2914, 2000.

Farley, K. A., R. A. Wolf, and L. T. Silver, The effects of long alpha-stopping distances on (U-Th)/He ages, *Geochim. Cosmochim. Acta*, *60*, 4223–4229, 1996.

Grove, M., and T. M. Harrison, ^{40}Ar* diffusion in Fe-rich biotite, *Am. Mineral.*, *81*, 940–951, 1996.

Hacker, B. R., E. Gnos, L. Ratschbacher, L. Webb, M. Grove, M. McWilliams, and W. Jiang, Hot and dry xenoliths from the lower crust of Tibet, *Science*, *287*, 2463–2466, 2000.

Hames, W. E., and B. C. Burchfiel, Laser ^{40}Ar/^{39}Ar dating of Cenozoic, greenschist-facies shear zones, Longmenshan, China, *Geol. Soc. Am. Abstr. Programs*, *25*, A118, 1993.

Harrison, T. M., P. Copeland, W. S. F. Kidd, and A. Yin, Raising Tibet, *Science*, *255*, 1663–1670, 1992.

Harrison, T. M., M. T. Heizler, and O. M. Lovera, In vacuo crushing experiments and K-feldspar thermochronometry, *Earth Planet. Sci. Lett.*, *117*, 169–180, 1993.

Harrison, T. M., M. T. Heizler, O. M. Lovera, W. Chen, and M. Grove, A chlorine disinfectant for excess argon released from K-feldspar during step heating, *Earth Planet. Sci. Lett.*, *123*, 95–104, 1994.

Hodges, K. V., W. E. Hames, W. Olszewski, B. C. Burchfiel, L. H. Royden, and Z. Chen, Thermobarometric and ^{40}Ar/^{39}Ar geochronologic constraints on Eohimalayan metamorphism in the Dinggye area, southern Tibet, *Contrib. Mineral. Petrol.*, *117*, 151–163, 1994.

House, M. A., and K. V. Hodges, Limits on the tectonic significance of rapid cooling events in extensional settings: Insights from the Bitterroot metamorphic core complex, Idaho-Montana, *Geology*, *22*, 1007–1010, 1994.

House, M. A., B. P. Wernicke, K. A. Farley, and T. A. Dumitru, Cenozoic thermal evolution of the central Sierra Nevada, California, from (U-Th)/He thermochronometry, *Earth Planet. Sci. Lett.*, *151*, 167–179, 1997.

House, M. A., B. P. Wernicke, and K. A. Farley, Dating topography of the Sierra Nevada, California, using apatite (U-Th)/He ages, *Nature*, *396*, 66–69, 1998.

House, M. A., K. A. Farley, and D. Stockli, Helium chronometry of apatite and titanite using Nd-YAG laser heating, *Earth Planet. Sci. Lett.*, *183*, 365–368, 2000.

Houseman, G. A., D. P. McKenzie, and P. Molnar, Convective instability of a thickened boundary layer and its relevance for the thermal evolution of continental convergent belts, *J. Geophys. Res.*, *86*, 6115–6132, 1981.

King, R. W., F. Shen, B. C. Burchfiel, L. H. Royden, E. Wang, Z. Chen, Y. Liu, X. Zhang, J. Zhao, and Y. Li, Geodetic measurement of crustal motion in southwest China, *Geology*, *25*, 179–182, 1997.

Kirby, E., Structural, thermal and geomorphic evolution of the eastern margin of the Tibetan Plateau, Ph.D. thesis, 211 pp., Mass. Inst. of Technol., Cambridge, 2001.

Kirby, E., and K. X. Whipple, Patterns of exhumation and rock uplift along the eastern margin of the Tibetan Plateau inferred from thermochronology and bedrock river incision, *Eos Trans. AGU*, *81*(48), Fall Meet. Suppl., Abstract T52F-03, 2000.

Kirby, E., K. X. Whipple, B. C. Burchfiel, W. Tang, G. Berger, Z. Sun, and Z. Chen, Neotectonics of the Min Shan, China: Implications for mechanisms driving Quaternary deformation along the eastern margin of the Tibetan Plateau, *Geol. Soc. Am. Bull.*, *112*, 375–393, 2000.

Krol, M. A., P. K. Zeitler, G. Poupeau, and A. Pecher, Temporal variations in the cooling and denudation history of the Hunza plutonic complex, Karakoram Batholith, revealed by ^{40}Ar/^{39}Ar thermochronology, *Tectonics*, *15*, 403–415, 1996.

Leloup, P. H., T. M. Harrison, F. J. Ryerson, W. Chen, O. Li, P. Tapponnier, and R. Lacassin, Structural, petrological, and thermal evolution of a Tertiary ductile strike-slip shear zone, Diancang Shan, Yunnan, *J. Geophys. Res.*, *98*, 6715–6743, 1993.

Lenardic, A., and W. M. Kaula, More thoughts on convergent plateau formation and mantle dynamics with regard to Tibet, *J. Geophys. Res.*, *100*, 15,193–15,203, 1995.

Lippolt, H. J., M. Leitz, R. S. Wernicke, and B. Hagedorn, (Uranium+thorium)/helium dating of apatite: Experience with samples from different geochemical environments, *Chem. Geol.*, *112*, 179–191, 1994.

Lovera, O. M., Computer programs to model ^{40}Ar/^{39}Ar diffusion data from multidomain samples, *Comput. Geosci.*, *7*, 789–813, 1992.

Lovera, O. M., F. M. Richter, and T. M. Harrison, The ^{40}Ar/^{39}Ar geothermometry for slowly cooled samples having a distribution of diffusion domain sizes, *J. Geophys. Res.*, *94*, 17,917–17,935, 1989.

Lovera, O. M., F. M. Richter, and T. M. Harrison, Diffusion domains determined by ^{39}Ar released during step heating, *J. Geophys. Res.*, *96*, 2057–2069, 1991.

Lovera, O. M., M. Grove, T. M. Harrison, and K. I. Mahon, Systematic analysis of K-feldspar ^{40}Ar/^{39}Ar step-heating experiments, I, Significance of activation energy determinations, *Geochim. Cosmochim. Acta*, *61*, 3171–3192, 1997.

Mancktelow, N. S., and B. Grasemann, Time-dependent effects of heat advection and topography on cooling histories during erosion, *Tectonophysics*, *270*, 167–195, 1997.

Mattauer, M., M. Matte, J. Malavieille, P. Tapponnier, H. Maluski, Z. Q. Xu, Y. L. Lu, and Y. Q. Tang, Tectonics of the Qinling Belt: Build-up and evolution of eastern Asia, *Nature*, *317*, 496–500, 1985.

McCaffrey, R., and J. Nabelek, Role of oblique convergence in the active deformation of the Himalayas and southern Tibet plateau, *Geology*, *26*, 691–694, 1998.

Meyer, B., P. Tapponnier, L. Bourjot, F. Metivier, Y. Gaudemer, G. Peltzer, S. Guo, and Z. Chen, Crustal thickening in Gansu-Qinghai, lithospheric mantle subduction, and oblique, strike-slip controlled growth of the Tibet plateau, *Geophys. J. Int.*, *135*, 1–47, 1998.

Ministry of Geology and Mineral Resources, G.M., *Regional Geology of Sichuan Province*, 728 pp., Geol. Publ. House, Beijing, 1991.

Molnar, P., P. England, and J. Martinod, Mantle dynamics, uplift of the Tibetan Plateau, and the Indian monsoon, *Rev. Geophys.*, *31*, 357–396, 1993.

Moore, M. A., and P. C. England, On the inference of denudation rates from cooling ages of minerals, *Earth Planet. Sci. Lett.*, *185*, 265–284, 2001.

Murphy, M. A., A. Yin, T. M. Harrison, S. B. Durr, Z. Chen, F. J. Ryerson, W. S. F. Kidd, X. Wang, and X. Zhou, Did the Indo-Asian collision alone create the Tibetan Plateau?, *Geology*, *25*, 719–722, 1997.

Parsons, I., D. C. Rex, P. Guise, and A. N. Halliday, Argon-loss by alkali feldspars, *Geochim. Cosmochim. Acta*, *52*, 1097–1112, 1988.

Parsons, I., W. L. Brown, and J. V. Smith, ^{40}Ar/^{39}Ar thermochronology using alkali feldspars: Real thermal history or mathematical mirage of microtexture?, *Contrib. Mineral. Petrol.*, *136*, 92–110, 1999.

Raymo, M. E., W. F. Ruddiman, and P. N. Froelich, Influence of late Cenozoic mountain building on ocean geochemical cycles, *Geology*, *16*, 649–653, 1988.

Reiners, P. W., K. A. Farley, and H. J. Hickes, He diffusion and (U-Th)/He thermochronometry of zircon: Initial results from Fish Canyon Tuff and Gold Butte, Nevada, *Tectonophysics*, in press, 2002.

Roddick, J. C., R. A. Cliff, and D. C. Rex, The evolution of excess argon in Alpine biotites — A ^{40}Ar/^{39}Ar analysis, *Earth Planet. Sci. Lett.*, *48*, 185–208, 1980.

Roger, F., S. Calassou, J. Lancelot, J. Malavieille, M. Mattauer, Z. Xu, Z. Hao, and L. Hou, Miocene emplacement and deformation of the Konga Shan granite (Xianshui He fault zone, west Sichuan, China): Geodynamic implications, *Earth Planet. Sci. Lett.*, *130*, 201–216, 1995a.

Roger, F., S. Calassou, J. R. Lancelot, J. Malavieille, and M. Mattauer, Geochronology and isotope geo-

chemistry of granitoids associated with the Songpan-Garze decollement (eastern Tibet), *Terra Abstr.*, *7*, 351–352, 1995b.

Royden, L., Coupling and decoupling of crust and mantle in convergent orogens: Implications for strain partitioning in the crust, *J. Geophys. Res.*, *101*, 17,679–17,705, 1996.

Royden, L. H., B. C. Burchfiel, R. W. King, Z. Chen, F. Shen, and Y. Liu, Surface deformation and lower crustal flow in Eastern Tibet, *Science*, *276*, 788–790, 1997.

Ruppel, C., L. Royden, and K. Hodges, Thermal modeling of extensional tectonics: Application to pressure-temperature-time histories of metamorphic rocks, *Tectonics*, *7*, 947–957, 1988.

Samson, S. D., and E. C. Alexander, Calibration of the interlaboratory $^{40}Ar/^{39}Ar$ dating standard, MMhb-1, *Chem. Geol.*, *66*, 27–34, 1987.

Seeber, L., and A. Pecher, Strain partitioning along the Himalayan arc and the Nanga Parbat antiform, *Geology*, *26*, 791–794, 1998.

Sengor, A. M. C., A. Cin, D. B. Rowley, and S. Y. Nie, Space-time patterns of magmatism along the Tethysides, *J. Geol.*, *101*, 51–84, 1993.

Spotila, J. A., K. A. Farley, and K. Sieh, Uplift and erosion of the San Bernardino Mountains associated with transpression along the San Andreas fault, California, as constrained by radiogenic helium thermochronometry, *Tectonics*, *17*, 360–378, 1998.

Stuwe, K., L. White, and R. Brown, The influence of eroding topography on steady-state isotherms: Application to fission track analysis, *Earth Planet. Sci. Lett.*, *124*, 63–74, 1994.

Tang, R., D. Wen, Z. Huang, X. Wu, W. Lin, G. Chen, and G. Wu, The Quaternary activity characteristics of several major active fault zones in the Songpan-Longmenshan region, *Earthquake Res. China*, *7*, 341–350, 1993.

Tapponnier, P., G. Peltzer, A. Y. Le Dain, R. Armijo, and P. Cobbold, Propagating extrusion tectonics in Asia: New insight from simple experiments with plasticine, *Geology*, *10*, 611–616, 1982.

Turner, S., C. Hawkesworth, J. Liu, N. Rogers, S. Kelley, and P. van Calsteren, Timing of Tibetan uplift constrained by analysis of volcanic rocks, *Nature*, *364*, 50–54, 1993.

Turner, S., N. Arnaud, J. Liu, N. Rogers, C. Hawkesworth, N. Harris, S. Kelley, P. van Calsteren, and W. Deng, Post-collisional, shoshonitic volcanism on the Tibetan Plateau: Implications for convective thinning of the lithosphere and the source of ocean island basalts, *J. Petrol.*, *37*, 45–71, 1996.

Villa, I. M., Multipath Ar transport in K-feldspar deduced from isothermal heating experiments, *Earth Planet. Sci. Lett.*, *122*, 393–401, 1994.

Wang, E., B. C. Burchfiel, L. H. Royden, L. Chen, J. Chen, W. Li, and Z. Chen, *Late Cenozoic Xianshuihe-Xiaojiang, Red River, and Dali Fault Systems of Southwestern Sichuan and Central Yunnan, China*, *Geol. Soc. Am., Spec. Pap.*, *327*, 108 pp., 1998.

Warnock, A. C., and P. K. Zeitler, $^{40}Ar/^{39}Ar$ thermochronometry of K-feldspar from the KTB borehole, Germany, *Earth Planet. Sci. Lett.*, *158*, 67–79, 1998.

Warnock, A. C., P. K. Zeitler, R. A. Wolf, and S. C. Bergman, An evaluation of low-temperature apatite U-Th/He thermochronometry, *Geochim. Cosmochim. Acta*, *61*, 5371–5377, 1997.

Willett, S. D., Inverse modeling of annealing of fission tracks in apatite,1, A controlled random search method, *Am. J. Sci.*, *297*, 939–969, 1997.

Willett, S. D., Orogeny and orography: The effects of erosion on the structure of mountain belts, *J. Geophys. Res.*, *104*, 28,957–28,981, 1999.

Wolf, R. A., The development of the (U-Th)/He thermochronometer, 211 pp., Calif. Inst. of Technol., Pasadena, 1997.

Wolf, R. A., K. A. Farley, and L. T. Silver, Helium diffusion and low-temperature thermochronometry of apatite, *Geochim. Cosmochim. Acta*, *60*, 4231–4240, 1996.

Wolf, R. A., K. A. Farley, and L. T. Silver, Assessment of (U-Th)/He thermochronometry: The low-temperature history of the San Jancinto mountains, California, *Geology*, *25*, 65–68, 1997.

Wolf, R. A., K. A. Farley, and D. M. Kass, Modeling of the temperature sensitivity of the apatite (U-Th)/He thermochronometer, *Chem. Geol.*, *148*, 105–114, 1998.

Xu, G., and P. Kamp, Tectonics and denudation adjacent to the Xianshuihe Fault, eastern Tibetan Plateau: Constraints from fission track thermochronology, *J. Geophys. Res.*, *105*, 19, 231–19,251, 2000.

Zeitler, P. K., Inversion of $^{40}Ar/^{39}Ar$ age spectra using the controlled-random-search method, *Eos Trans. AGU74*(43), Fall Meet. Suppl., F650, 650, 1993.

Zeitler, P. K., A. L. Herczeg, I. McDougall, and M. Honda, U-Th-He dating of apatite: A potential thermochronometer, *Geochim. Cosmochim. Acta*, *51*, 2865–2868, 1987.

Zhou, D., and S.A. Graham, Songpan-Ganzi complex of the west Qilian Shan as a Triassic remnant ocean basin, in *The Tectonic Evolution of Asia*, edited by A. Yin and T. M. Harrison, pp. 281–299, Cambridge Univ. Press, New York, 1996.

Z. Chen and W. Tang, Chengdu Institute of Geology and Mineral Resources, 82 North-3 Section, First Ring Road, Chengdu, Sichuan, P.R. China. (zhilchen@mail.sc.cninfo.net)

K. A. Farley, Department of Geological and Planetary Sciences, California Institute of Technology, MS 170-25, 391 S. Holliston Avenue, Pasadena, CA 91125, USA. (farley@gps.caltech.edu)

K. V. Hodges and K. X. Whipple, Department of Earth, Atmospheric, and Planetary Science, Massachusetts Institute of Technology, Room 54-1120, Cambridge, MA 02139, USA. (kvhodges@mit.edu; kxw@mit.edu)

E. Kirby, Institute for Crustal Studies, University of California, Santa Barbara, CA 93106, USA. (ekirby@crustal.ucsb.edu)

M. A. Krol, Department of Earth Sciences, Boston University, Boston, MA 02215, USA. (mkrol@bridgew.edu)

P. W. Reiners, Department of Geology and Geophysics, Yale University, New Haven, CT 06520, USA. (pwr2@morpheus.its.yale.edu)